OPTICAL, ELECTRICAL AND STRUCTURAL PROPERTIES OF ZINC STANNATE (Zn_2SnO_4) THIN FILMS PREPARED BY SPRAY PYROLYSIS TECHNIQUE.

THIS THESIS HAS BEEN ACCEPTED FOR THE DEGREE OF MSC 1997

BY

JOSEPH MULIARO WAFULA, *B.SC. (HONS.)*

A THESIS SUBMITTED IN PARTIAL FULFILMENT OF THE REQUIREMENT FOR THE DEGREE OF MASTER OF SCIENCE IN PHYSICS AT THE UNIVERSITY OF NAIROBI.

APRIL 1997

This thesis is my original work and has not been presented for a degree in any other university.

Joseph muliaro Wafula

Department of Physics

University of Nairobi

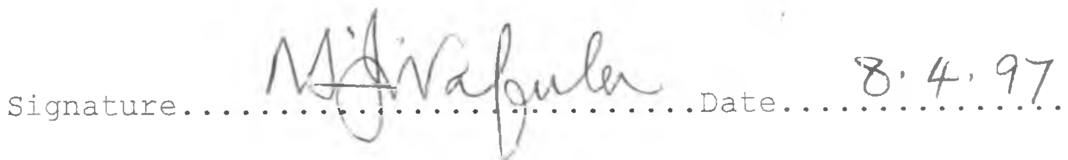

Signature.............................Date.. 8.4.97

This thesis has been submitted for examination with our approval as university supervisors.

Dr. A.K. Raturi

Department of Physics

University of Nairobi

Signature.............................Date. 9th April 97

Dr. B.O. Aduda

Department of Physics

University of Nairobi

Signature.............................Date. 9th April 1997

DEDICATION

This thesis is dedicated to my parents Julius Sindani Wafula and Peninah Ajiambo Wafula in recognition of their wisdom and support for my adventure in academic career which I have found promising. May God multiply thier blessing.

TABLE OF CONTENTS

Declaration i

Dedication ii

List of Symbols vi

List of Tables x

List of Figures xi

List of Appendices xiii

Acknowledgements xiv

Abstract xv

CHAPTER ONE

1.0 INTRODUCTION 1

1.1 Solar Energy and Transparent Conductors ... 1

1.2 Objectives of the Research 3

CHAPTER TWO

2.0 LITERATURE REVIEW 4

2.1 Introduction 4

2.2 Zinc Oxide (ZnO) Thin Films 4

2.3 Tin Oxide (SnO_2) Thin Films 7

2.4 Other Transparent Conductors 10

2.5 Summary 11

CHAPTER THREE

3.0 THEORETICAL BACKGROUND 13

3.1 Crystal Growth 13

3.2 Crystallography and Crystal Defects 14

3.3 Stress in Thin Films 17

3.4 Recombination Mechanisms 18

3.4.1 Recombination Through Traps 19

3.4.2 Surface Recombination 21

3.5 Band Shapes of Semiconductors 21

3.6 Electronic States 24

3.7 Fundamental Electronic Absorption 25

3.8 Transmission and Reflection 28

3.9 Figure of Merit for Transparent Conductors .. 29

CHAPTER FOUR

4.0 EXPERIMENTAL TECHNIQUES 31

4.1 Introduction 31

4.2 Experimental Set-Up 34

4.2.1 Film Growth 34

4.3 Transmission and Sheet Measurements 37

4.4 Annealing Studies 37

4.5 Determination of Band Gap 37

4.6 Film Thickness Measurement 38

4.7 Hall Effect Studies 39

4.8 Structural and Topographic Studies............ 41

CHAPTER FIVE

5.0 RESULTS AND DISCUSSION........................ 42

5.1 Optimization of Growth Parameters............. 42

5.2 Sructural Properties of Zn_2SnO_4 Films 45

5.2.1 Surface Topography 45

5.2.2 X-Ray Diffraction Studies 45

5.3 Optical Properties............................. 48

5.3.1 Transmission Spectra 48

5.3.2 Absorption Coefficient........................ 51

5.3.3 Extinction Coefficient........................ 55

5.3.4 Band Gap 58

5.4 Annealing Studies............................. 62

5.5 Hall Effect Studies 67

5.6 Figure of Merit 67

CHAPTER SIX

6.0 CONCLUSION AND SUGGESTION FOR FURTHER WORK..... 69

6.1 Conclusion 69

6.2 Suggestion for Further Work.................. 70

7 **REFERENCES** 71

8 **APPENDICES** 74

LIST OF SYMBOLS IN THE MAIN TEXT

B_z - magnetic field in z-direction.

C_n - capture rate per electron when all traps are empty.

C_p - capture rate per hole when all traps are empty.

d - deflection of substrate.

d_s - stop distance.

E_f - final electron state energy.

E_i - initial electron state energy.

E_g - band gap energy.

E_s - Fermi energy.

E_x - electric field in x-direction.

F_s - Stoke's force.

F_t - fraction of traps occupied by electrons.

g - acceleration due to gravity.

h - Planck's constant.

I_y - current in y-direction.

k - extinction coefficient.

k - photon momentum

$\mathbf{k_f}$ - final photon momentum.

$\mathbf{k_i}$ - initial photon momentum.

K - phonon momentum.

K_a - air thermal conductivity

k_B - Boltzmann constant

K_d - aerosol droplet thermal conductivity

L - length of film

L_s - length of substrate

m - mass

m_n - number of maxima

n - number of electrons

n_1 - number of electrons in conduction band when the Fermi level coincides with the trapping levl

n_r - refractive index

N - carrier concentration

p - number of holes

p_1 - number of holes in valence band when the Fermi level coincides with the trapping level

q - charge

r - radius

R - reflection coefficient at air-film interface

R_1 - reflection coefficient at film-substrate interface

R_c - capture rate

R_e - rate of emmission from traps

R_H - Hall coefficient

R_n - net trapping rate for electrons

R_p - net trapping rate for holes

R_{np} - constant rate of creation of electron-hole pairs

R_s - sheet resistance

R_{si} - initial sheet resistance

t - film thickness

t_s - substrate thickness

Δt - two films thickness difference

T - temperature

ΔT - temperature difference between film growth and measurement

ΔT_a - air thermal gradient

T_o - transmission

T_{1-2} - transmission ratio

V_a - air velocity

V_d - drop velocity

V_H - Hall voltage

V_o - stop velocity

Y_F - Young's modulus of film

Y_s - Young's modulus of substrate

α - absorption coefficient

α_F - thermal expansion coefficient of film

α_s - thermal expansion coefficient of substrate

σ - electrical conductivity

σ_s - film stress

σ_{th} - thermal stress

ρ - resistivity

ρ_a - air density

μ - mobility

μ_p - Poisson's ratio

ϕ - angle of incidence

ϕ_{TC} - figure of merit

τ - relaxation time

ν - photon frequency

v_n - phonon frequency

π - pi

$-$ - subtraction

$+$ - addition

$>$ - greater than

$<$ - less than

LIST OF TABLES

Title Page

Table 1 : Values of transmission (T_2), wavelength (λ), absorption coefficient (α) and photon energy ($h\nu$) for Zn_2SnO_4 film of thickness 1592.6 Å 53

Table 2 : Value of wavelength (λ), extinction coefficient (k) and photon energy ($h\nu$) for Zn_2SnO_4 films of thickness 1592.6 Å and refractive index 2 56

Table 3 : Values of relative Transmission (T_{1-2}), wavelength (λ), $(h\nu\alpha\Delta t)^2$, photon energy ($h\nu$) and $\alpha\Delta t$ used to determine band gap 60

Table 4 : Natural logarithm of sheet resistance and reciprocal of temperature for vacuum annealed Zn_2SnO_4 films 65

Table 5 : Values of substrate temperature (T), resistivity (ρ), carrier concentration (N) and mobility (μ) for the best Zn_2SnO_4 sample studied 67

Table 6 : Hall effect data and results for Zn_2SnO_4 thin films grown at different substrate temperatures. 76

LIST OF FIGURES

Title	Page
Fig. 3.1 : The energy band in momentum space for (a) indirect band gap semiconductor (Si) and (b) direct band gap semiconductor (GaAs)	23
Fig. 3.2 : (a) shows a direct band gap semiconductor, such as GaAs. (b) shows an indirect band gap semiconductor, such as Si	27
Fig. 4.1 : Experimental set-up for spray pyrolysis technique	36
Fig. 4.2 : Hall effect measurements set-up	40
Fig. 5.1 : Variation of sheet resistance with substrate temperature	44
Fig. 5.2 : Scanning electron micrographs of vacuum annealed Zn_2SnO_4 films with substrate temperature of (a) 380 °C and (b) 440 °C	46
Fig. 5.3 : X-ray diffraction pattern for zinc stannate films grown at (a) 380 °C and (b) 440 °C	47
Fig. 5.4 : Transmission spectra for zinc stannate films grown at (a)350 °C, (b) 400 °C and (c) 440°C	49

Title	Page

Fig. 5.5 : Transmission spectra for (a) as-deposited zinc stannate films and (b) after annealing in vacuum.................................. 50

Fig. 5.6 : Interference fringes 52

Fig. 5.7 : Absorption coefficient Vs. wavelength 54

Fig. 5.8 : Extinction coefficient Vs. photon energy...... 57

Fig. 5.9 : Transmission spectrum of a thicker film relative to a thinner zinc stannate film...... 59

Fig. 5.10 : Determination of band gap 61

Fig. 5.11 : Variation in sheet resistance with temperature of zinc stannate films on annealing in different ambients. The annealing steps in chronological order were as labelled curves a - b, where the curves represent:

a - annealing in air with increase in temperature

b - annealing in vacuum at constant temperature

b - cooling in air

d - annealing in vacuum with increase in temperature..63

Title Page

Fig. 5.12 : In (R_s) Vs reciprocal temperature for zinc stannate films.............................. 66

LIST OF APPENDICES

Title Page

Appendix A : Film thickness calculations 74

Appendix B : Absorption coefficient calculations 75

Appendix C : Hall effect studies calculations 76

ACKNOWLEDGEMENTS

A number of persons and institutions have contributed to the realization of this thesis. I wish to thank them for their help. In particular I am very grateful to Dr. Raturi and Dr. Aduda for their indispensable supervision of this thesis. Likewise, I am also grateful to the Japanese International Co-operation Agency (JICA) for awarding me a scholarship that enabled me pursue M.Sc. program. To my sister Irene and brother Peter, I am at a loss of words to thank them for the special company and fellowship they gave me particularly during M.Sc. Part I (course-work and examinations), that immensely contributed to my excellent performance. May God bless them, and bless too those who remembered me in prayers.

ABSTRACT

Highly transparent and conducting Zn_2SnO_4 films have been prepared by spray pyrolysis technique. Films grown at a substrate temperature of 440 ^0C exhibit the best optical and electrical properties. The microcrystals of these films had a preferred orientation along c-axis normal to the surface. The direct band gap was found to be 3.1 eV. Hall effect studies on these films yielded a carrier concentration of $1.2x10^{2}$[illegible] cm^{-3} and a mobility of 2.5 $cm^2/V.sec$. These films have a potential to perform as good transparent conductors and can be used in solar energy devices such as solar cells and solar collectors.

CHAPTER ONE

1.0 INTRODUCTION

1.1 Solar Energy and Transparent Conductors

Solar energy sustains life on earth. Fossil fuels have limited reserves and may be exhausted soon. Nuclear fuel is in abundance and clean in terms of environment-green house gas and global warming, but has its disadvantages e.g. nuclear waste disposal. Solar energy is inexhaustible, clean and environmentally friendly. It is pollution free and not harzadous chemically. Solar energy is also independent of political and geographical boundaries [1].

Utilization of solar energy can be divided into two categories: these are photothermal and photovoltaic. In both photothermal and photovoltaic systems, optical, structural and electrical properties have significant effects on the overall performance of the system. Wide spread utilization of solar energy requires the development of durable, low cost and optically efficient solar selective coatings. For transparent conducting coatings, one can either use a metal with high infrared reflectivity and very low visible absorption or a semiconductor with a wide band gap sufficiently wide to be transparent in the visible range and a high enough carrier concentration to have high infrared reflectivity [2]. The increasing use of transparent conducting films for solid state display devices, solar cells, and transmittance-variable glazing has promoted the development of inexpensive materials like zinc oxide and tin oxide, in place of

indium tin oxide (ITO). The desired properties of a transparent conducting film are a high band gap (above 3.0 eV), and a low effective mass of charge carriers and high carrier mobility. Recently, ZnO:Al films have been actively investigated as a transparent conducting material in place of ITO and it has been realized that their electrical resistivity differ with the morphological structure of the film [3].

The electrical and optical properties of transparent conducting films depend mainly on the preparation method and the oxidation state i.e., undoped In_2O_3 films prepared by simple reactive ion plating technique possessed remarkable electrical and optical properties of resistivity less than $1.5x10^{-4}$ Wcm and high visible transmission (over 90%) respectively [4]. Post annealing of amorphous films results into polycrystalline films. The high crystallinity is confirmed by x-ray diffraction (XRD) [6].

Examples of materials which on doping become transparent conductors are all oxides based on zinc, cadmium, indium, tin, thallium, and lead and their alloys. Particularly good properties have been obtained with SnO_2:F, SnO_2:Sb, InO_3:Sn, ZnO:Al, Cd_2SnO_4 e.t.c.[7]. These transparent conductors can find their application in photovoltaic systems. Photovoltaic systems generate electricity without emitting green house gases and result in global, regional and local air quality advantages. Photovoltaic systems used in rural applications often replace kerosene lamps with electric lights. Solar-based rural electrification can provide a source of employment, hence an

increase in commercial activity and productivity (e.g. agricultural, through solar powered water pumps).

Other stannates e.g. cadmium stannate have been studied however, there is lack of information on zinc stannate as a transparent conductor and its application as a solar selective coating. We thus aim to study structural, optical and electrical properties of zinc stannate prepared by spray pyrolysis technique. It has been found that the spray technique is most suitable for obtaining films of high optical transmission and low sheet resistance. Further, spray technique is inexpensive and ideally suitable for large area substrate application [8].

1.2 Objective of the Research

The objectives of the research were :

1. To grow zinc stannate (Zn_2SnO_4) thin films using spray pyrolysis technique,
2. To optimize deposition parameters for low sheet resistance and high transmittance zinc stannate thin films and
3. To study the structural, electrical and optical properties of zinc stannate thin films.

CHAPTER TWO

2.0 LITERATURE REVIEW

2.1 Introduction

Transparent and conducting thin films have been investigated by many researchers. Several techniques have been used i.e. spray pyrolysis [8,9,10,11], Dual-ion-beam sputtering [12], rf magneton sputtering [3,10,13,14], organometallic chemical vapour deposition (OMCVD) [15], reactive ion plating [4], metalorganic chemical vapour deposition (MOCVD) [16], dc magneton sputtering [17], sputtering [18,19,20], highly dense plasma-assisted EB evaporation (HDPE) [6] and laser photochemical deposition [21].

2.2 Zinc Oxide (ZnO) Thin Films

ZnO films deposited by ion-beam sputtering (IBS) are clear and transparent. No spell, crack, or microscopic sign of stress and poor adhesion are detected on the samples. X-ray-diffraction measurements indicate that most ZnO films prepared by (IBS) technique prefer an orientation with c-axis normal to the substrate. Diffraction peaks shift to lower values than those for monocrystals. This shift is due to an in-plane compression stress that produces an increase of crystalline plane distance in the growth direction. ZnO films prepared by (IBS) techniques give an optical band gap of about 3.26 eV and resistivity between 10^{-5} and 10^{5} Ωcm depending on chosen conditions [12].

ZnO thin films exhibit strong piezoelectric and piezo-optic effects and have often been used in acoustoelectric and acousto-optic (AO) devices such as surface acoustic wave (SAW) filters and AO Bragg deflectors. A strong causal relationship exist between the optical properties and the crystallographic properties of ZnO films. Only (002) and (004) diffraction peaks are seen in ZnO films. An increase of substrate temperature promotes the c-axis orientation of ZnO films, although overheating of the substrate causes a negative influence on the crystallographic properties. ZnO films with good optical properties is obtained by a film with good orientation and a high density. The improvement of the optical property can be attributed to the films with good orientation (i.e. little surface roughness and low scattering) and the films with high density, which is due to the uniformity in optical property such as refractive index [5].

The size of crystallites and the magnitude of the associated grain-boundary effects depend upon the method used to prepare the film. ZnO film prepared by the oxidation of diethyl zinc is n-type wide-band-gap semiconductor. It has a band gap of 3.3 eV at room temperature. It is generally accepted that in undoped nonstoichometric ZnO film the n-type conductivity is due the oxygen deficiencies and interstitial zinc. The electrical properties are influenced by the size and orientation of crystallites and by the grain boundary characteristics. Chemisorption of oxygen occurs on ZnO and is removed through a desorption process where UV illumination is done under vacuum.

Rapid decrease in conductivity occur immediately the film is allowed to stand in air followed by a slower but much larger decrease. These effects are consistent with first, a surface effect followed by a slower change due to diffusion through the grain boundaries [15].

The use of ZnO layer with GaAs substrate enables one to monolithically integrate surface acoustic wave (SAW) devices with GaAs electronics. C-axis oriented polycrystalline ZnO films are grown by rf magneton and dc triode sputtering methods [13]. Over the past two decades, ZnO has been the most frequently considered piezoelectric thin film material for use in increasing the piezoelectric coupling in cases where weakly or non piezoelectric substrates are employed [14]. Annealed ZnO films prepared by sputtering, give sharp x-rays diffraction peaks that shift to the right. Highly c-oriented, bigger crystallite size, and reduced-stress ZnO films are obtained after heat treatments [18].

Electrical properties of ZnO:Al films are affected by adsorption of oxygen on their surface. Resistivity of ZnO:Al films as a function of substrate temperature, decreases to a minimum value about 1.5×10^{-4} Ωcm at 150 °C and then increase again with temperature [3]. The resistivity is proportional to the reciprocal of the product of the carrier concentration and the mobility. In ZnO:Al films, two kinds of donors are considered. One consisting of interstitial Zn atoms or oxygen vacancies which are the so-called native donors and the other is composed of

substitutional aluminum atoms. Change in carrier concentration with substrate temperature is due to the change in number of native donors. The mobility of carriers is closely related to the macroscopic and microscopic imperfections in the ZnO:Al films. The macroscopic imperfections include grain boundary, internal stress, and surface roughness which can be observed from the x-ray diffraction spectrum and the microscopic ones imply the ionized donors and/or the neutral impurity atoms. Mobility depends on films thickness and surface roughness. Surface of ZnO:Al films grown at substrate temperature up to 350 C are relatively smooth but those grown at about 400 °C are very rough. A rapid increase in resistivity at substrate temperature of 400 °C is ascribed to the fact that the film surface became rough, resulting in an increase in the surface diffusivity and a decrease in the effective conducting path carriers [3].

2.3 Tin Oxide (SnO_2) Thin Films

Kameswara *et al* [9] prepared transparent conducting tin oxide films by spray pyrolysis technique that gave a transmittance of 80% - 90% and a resistivity close to 10^{-3} Ωcm. The growth rate of tin oxide films deposited by spray pyrolysis technique, improved when the droplets were transported to the substrate in an ideal way i.e., as the droplets approached the surface, the solvent in the droplets vaporized completely.

Monocrystalline SnO_2 epitaxial films are prepared using reactive sputter deposition technique. High enough deposition temperature

and low enough rates are needed for a step controlled growth Mechanism [19]. SnO_2 films deposited at room temperature on substrate, using an Arf (193nm) excimer laser to drive the photochemical reaction of mixed $Sncl_4$ and N_2O vapours, have resistivity as low as 0.04 Ωcm without any annealing. The optical band gap of 3.20 eV and transmission cutoff wavelength of 330 nm compared favorably with the best films obtained using alternate higher temperature techniques. Subsequent annealing does not increase the films conductivity [21].

SnO_2 is an n-type semiconductor material with a direct band gap of about 4.0 eV and an indirect band gap of about 2.6 eV. High transparency and conductivity of SnO_2 is obtained by doping it with fluorine, the direct band gap is about 4.1 eV and the electrical resistivity is in the order of $5.4x10^{-4}$ Ωcm [10]. Electron diffraction pattern of undoped and antimony-doped tin oxide films prepared using spray pyrolysis technique at 540 ^{0}C show that they are polycrystalline and are of tetragonal structure. A gradual decrease in the resistivity occurs on raising the temperature of deposition from 340 ^{0}C to 540 ^{0}C. On the other hand, the carrier concentration and mobility show an increase with substrate temperature, the variation in mobility being larger than the variation in carrier concentration. The small increase in carrier concentration in undoped tin oxide films with deposition temperature is attributed to the increase in number of oxygen vacancies. Grain boundary scattering is the dominant scattering mechanism limiting the mobility. The

dependence of the mobility on deposition temperature can be understood on the basis of grain boundary scattering. The grain size increases with deposition temperature, causing a concurrent decrease in grain boundary potential. Hence the grain boundary scattering reduces leading to an increase in mobility. Transmission in the wavelength range 0.4 to 1.0 μm for undoped tin oxide films remains high (80%). Plasma resonance occurs in the near infrared region owing to high concentration ($10^{20}/cm^{3}$) of free carriers in the films. The fundamental absorption edge shifts from 3.95 eV for a carrier concentration of $10^{18}/cm^{3}$ to 4.62 eV corresponding to a carrier concentration of $7.9x10^{20}cm^{3}$. The shift in the fundamental absorption edge can be attributed to the Moss-Burstein shift, which occurs owing to filling up of low lying energy levels by the conduction electron [8].

Antimony-doped tin oxide films grown along [200] have been observed to possess higher conductivity. The increase in carrier concentration with doping is due to the replacement of Sn atoms by an added Sb atom, which gives one extra charge carrier. At very high doping levels the decrease in carrier concentration is because of the possible existence of antimony atoms in Sb^{3+} state. Increase in mobility is due to reduction in grain boundary scattering. Reduction in mobility at higher dopant levels can possibly be attributed to ionized impurity scattering [11].

2.4 Other Transparent Conductors

Undoped In_2O_3 films prepared by simple reactive ion plating technique have low resistivity of less than 1.5×10^{-4} Ωcm and high visible transmission (over 90%) readily obtained without any post-deposition annealing. Sheet resistance (the dimensions of sheet resistance is customarily quoted in Ω/□ to indicate that it measures the resistance of a square surface area where by the square area is independent of dimension and absolute value) of In_2O_3 films decreases rapidly with substrate temperature, especially below 150 ^{0}C, and saturated at 10-20 Ω/□ around 250 ^{0}C. In_2O_3 films of low resistivity have smooth surfaces without hillocks which are usually observed on evaporated films [4].

GaN is a candidate for transparent conducting films because it is a direct band gap semiconductor with a band gap energy of 3.39 eV and high electron mobility at room temperature. Impurity doped GaN has high chemical and thermal stability [16]. Amorphous zinc-phosphide (Zn_3P_2) film is prepared by reactive rf sputtering of Zinc in PH_3 containing argon atmosphere. Stoichiometric Zn_3P_2 films grown at substrate temperature below 200 ^{0}C are noncrystalline while films grown at 300 ^{0}C are purely polycrystalline. Annealing for 2 hrs at 300 ^{0}C cause complete crystallization of Zn_3P_2 films. A shift of the absorption edge in amorphous semiconductor films is related to voids. Two major reasons for the displacement of the absorption edge of evaporated films may exist. First, different growth conditions such as the deposition rate or the substrate temperature might

influence the amount and dimension of voids present. Second, impurities present due to ambient gases might form bonds with dangling bonds on the void surfaces [20].

The average grain size of copper thin films increases with increasing annealing temperature, ranging from 0.11 to 0.35 μm for the normal growing to 1.32 μm for the abnormally growing grains in copper thin films. Annealing also increases the intensity of peaks [8].

Cadmium stannate is an n-type semiconductor in which oxygen vacancies are believed to provide the donor states. A large Burstein shift also has been observed in the optical spectra, which indicate a low free carrier effective mass. Cd_2SnO_4 crystallizes in the orthorhombic structure. Nearly stoichiometric films have a low band gap of 2.06 eV leading to an absorption edge in the middle of the visible spectrum. Cd_2SnO_4 stoichiometric films can be obtained with minimum resistivity of $3x10^{-4}$ Ωcm. Sputtered crystalline Cd_2SnO_4 films contain CdO and $CdSnO_3$ phases which can be avoided by adjusting the deposition conditions. A sheet resistance of 1 Ω/□ and 85% average transmission at 5500 A has been achieved [2].

2.5 Summary

The growth rate of films deposited by spray pyrolysis technique is improved when the droplets are transported to the substrate in an ideal way i.e. as the droplets approach the surface, the

solvent in the droplet vaporizes completely [9]. Annealing of deposited films improves their crystallization, grain sizes and also sharpen peaks observed on x-ray diffraction chart [8,18,20].

Films with good orientation (i.e. little surface roughness and low scattering) and a high density (uniformity in optical property such as refractive index) have good optical properties [5]. Conductivity in undoped transparent conducting thin films is mainly due to oxygen deficiencies [8,15]. Shanthi *et al* [8], observed that grain boundary scattering is the dominant scattering mechanism limiting mobility. Whereas the mobility of carriers is closely related to the macroscopic (e.g. grain boundary and surface roughness) and macroscopic (e.g. ionized donors and/or the neutral impurity atoms) imperfections [3]. The size and orientation of the crystallites as well as the grain boundary characteristics, influence the electrical properties of transparent conducting thin films [15].

Fundamental information revealed to us through literature review is crusial, for instance, the success and the limitations of spray pyrolysis technique has to be understood before attempting to achieve our first objective of depositing Zn_2SnO_4 thin films, followed by optimization of its growth parameters. Due to lack of literature on Zn_2SnO_4 thin films, it is vital that a good sample of e.g. ZnO, ZnO:Sn, SnO_2 and Cd_2SnO_4 transparent conductors be studied for comparison purposes with Zn_2SnO_4 films during characterization.

CHAPTER THREE

3. THEORETICAL BACKGROUND

3.1 Crystal Growth

The majority of solids produced in nature are grossly imperfect and impure, a direct result of the haphazard way in which they are formed. Thus the first stage in producing a semiconductor device is the purification of the material and then the growth of high-quality single crystal under controlled and ultra-clean conditions. Techniques of crystal growth have in resent years proliferated, each material having demanded its own variation to overcome its particular problems.

Bulk-grown crystals of a quality sufficiently good for direct device fabrication are difficult to grow. One way of circumventing this difficulty is to use a polished slice of bulk grown crystal as a foundation and to grow on to this surface a much higher-grade epitaxial layer for the actual device structures. The word epitaxial means that the new crystal layer has the same crystal structure as the base wafer.

Liquid Phase Epitaxy (LPE) process involves a substrate (seed) crystal held above a semiconductor melt and then dipped into it. As the substrate is withdrawn from the melt to the cooler region of the furnace, the molten film covering the surface

will form an epitaxial crystal line layer provided the rate of cooling is carefully controlled.

The basis of Molecular Beam Epitaxy (MBE) technique is to allow a beam of the desired constituent atoms to fall upon, and stick to, a desired substrate held at an elevated temperature in ultra-high vacuum chosen such that it allows the best crystal to grow on the substrate [28].

In spray pyrolysis technique the prepared solution is first atomized to fine droplets. The droplets are then transported to the hot substrate where they undergo a suitable reaction to form crystalline films.

3.2 Crystallography and Crystalline Defects.

Defects in crystalline materials can be categorized as point defects, line defects, planar defects and volume defects. Although defects are generally undesirable and often unavoidable in crystal, in some cases they can be put to use to improve the device performance.

Point defects can be categorized as native defects such as vacancy and impurity related defects due to the introduction of an impurity atom into the lattice. For semiconductors, point defects not only cause structural disturbance, but also often introduce electronic states in the band gap. Three types of native defects are vacancy, interstitial and interstitialcy. Interstitial atoms, or interstitialcies, are atoms of the host

lattice. They may be foreign atoms or host atoms that have become misplaced.

Line defects are known as dislocations. In contrast to point defects, deslocations are formed due to nonequilbrium conditions such as thermal and mechanical processing and epitaxy. Space charge region forms around each dislocation, hence transport of the carrier normal to the dislocation lines would be affected due to winding current path, resulting in the increased resistivity and reduced carrier mobility. In addition to space-charge effects, dislocation may act as generation-recombination centres for carriers.

Planar defects include grain boundaries, stacking faults and twins. These defects are formed during crystal growth and/or during thermal and mechanical processing of semiconductors. A grain boundary may be viewed as an array of dislocations separating to single grains of crystalline material with a misorientation between them. Whereas Volume defects include voids and local regions of different phases, such as a precipitate or an amorphous phase [29].

Identification of the process controlling the incorporation of nature (or intrinsic) defects during semiconductor material preparation and/or processing is of primary importance since so many electronic and structural properties critically depend on the presence of such defects. The major aspects of the amphoteric defects concept as explained by Walukewicz [30], is

based on the discovery that the introduction of large-enough concentrations of native defects always leads to the same ultimate position of the Fermi energy, E_s . Walukewicz [30] has shown in a detailed analysis of the GaAs case that a new class of defects "amphoteric native defect" with Fermi energy-controlled formation energy and defect reaction rates are responsible for the stabilization of the Fermi level. The E_{FC} dependent reduction of the defect formation energy is the very property of the amphoteric native defects which is essential for the explanation of several previously poorly understood phenomena in semiconductors. This same concept can be used to understand doping-induced superlattice intermixing and limitation of free-carrier concentrations in semiconductors.

Surface crystal structure can be studied in the growth chamber using Low Energy Electron Diffraction (LEED) and Reflection High Energy Electron Diffraction (RHEED) instruments. Particles create structural defects in semiconductors and metal films grown by sputtering, evaporation and Molecular Beam Epitaxy (MBE) techniques. These defects have a variety of deleterious effect on device performance and on the process yield of integrated circuits. Many of these particles are assumed to originate in the vacuum equipment, and efforts are being made to reduce the defect density through better vacuum system design [31].

3.3 Stress in Thin Films.

The elastic stress present in thin films is an inherent part of the deposition process and can be either tensile or compressive. The sign and magnitude of the film stress depend on the processing parameter (i.e. substrate temperature, type of substrate, rate of decomposition, and method of deposition). Stress of about 10^8 to 10^9 N/m^2 are often observed in thin films. These stresses may cause film fracture, delamination, and occasionally, substrate fracture. Stress in a film consists of two major components, a "thermal" component arising from the difference in the thermal-expansion coefficients of the film and the substrate, and an "intrinsic" component resulting from the growth and the substrate of the film. The thermal component, called thermal stress, σ_{th} is given by [29]

$$\sigma_{th} = Y_F(\alpha_F - \alpha_S)\Delta T \qquad (3.1)$$

where Y_F is Young's modulus of the film, α_F and α_S are the thermal expansion coefficients of the film and the substrate respectively, and ΔT is the temperature of the substrate during film growth or deposition minus the temperature at measurement.

One of the most convenient ways to determine the stress in thin films is to measure the curvature of the film-substrate composite structure. The following expression derived from bending plate theory gives the stress σ_s in a film [29]

$$\sigma_s = \frac{dY_s t_s^2}{3L_s^3 t(1-\mu_p)}(1+\frac{Y_F t}{Y_s t_s}) \qquad (3.2)$$

where d is the deflection of the substrate, Y_F and Y_s are the Young's moduli of the film and the substrate respectively, t_s and t are the thickness of the substrate and the film, respectively, L is the length of the substrate and μ_p is Poisson's ratio.

If the stress in a thin film is higher than adhesion between the film and the substrate, delimination of the film occurs. If the stress in the film is higher than the fracture strength of the film but less than the film-substrate adhesion, the film itself may fracture. The stress in the thin-film structures is a critical parameter for the mechanical stability of the deposited layer [29].

3.4 Recombination Mechanisms

The recombination mechanisms may be divided into three main categories: (a) direct recombination, (b) recombination through traps and (c) surface recombination.

In direct recombination, the electrons and the holes combine through an electron dropping from a state in the conduction band to an empty state in the valence band in a single transition. An amount of energy in excess must be dessipated off by some means and the simplest process by which this can be done is by radiation.

Recombination through traps is one in which an electron makes the jump from the conduction band to the valence band in two steps, which may be separated by a relatively large amount of energy. For example, an electron may be captured into a deep trap whose energy lies near the middle of the forbidden energy gap; subsequently, the occupied trap may capture a hole and the recombination process will then be completed.

For surface recombination, the traps are now at the surface of the semiconductor.

3.4.1 Recombination Through Traps.

The capture rate (R_c) can be expressed as [33]

$$R_c = C_n n(1-f_t) \tag{3.3}$$

where n is the number of electrons, C_n is the capture rate per electron when all the traps are empty and f_f is the fraction of the traps occupied by electrons.

The rate of emission (R_e) from the traps can be expressed as [33]

$$R_e = n_1 C_n f_t \tag{3.4}$$

where n_1 is the number of electrons in the conduction band when the Fermi level coincides with the trapping level.

Therefore the net trapping rate for electrons (R_n) can be expressed as [33]

$$R_n = C_n[(1-f_t)n-n_1f_t] \tag{3.5}$$

similarly the net trapping rate for holes (R_p) may be written in the form [33]

$$R_p = C_p[f_tp-p_1(1-f_t)] \tag{3.6}$$

Where p is the number of holes, p_1 is the number of holes in the valence band when the Fermi level coincides with the trapping level.

If we now have a disturbing influence creating electron-hole pairs at a constant rate R_{np}, when steady conditions have been established, electrons and holes will be trapped at the same rate, since they recombine in pair, and we have

$$R_n = R_p = R_{np} \tag{3.7}$$

This gives us an equation for the f_t of traps which are occupied. We have on equating R_n and R_p [33]

$$f_t = \frac{nC_n + p_1C_p}{C_n(n-n_1)+C_p(p+p_1)} \tag{3.8}$$

3.4.2 Surface Recombination

In addition to recombination in the body of a semiconductor, electrons and holes may diffuse to the surface and recombine there, and, under some conditions, the rate of recombination at the surface may be much greater than the body recombination rate. Indeed, for many technological applications, special precautions must be taken to ensure that the surface recombination rate is not intolerably high; for example, if the surface recombination rate near a point contact is unduly high it may affect adversely the properties of the contact.

3.5 Band Shapes of Semiconductors

Fig 3.1 shows the valence and conduction band of two semiconductors. The curves are not symmetrical since different **k**-directions are used for each side, so as to show more than one crystal orientation and also the various minima in the conduction bands. It is in Fig 3.1(b) that the lowest conduction band minimum occur at **k**=0, but in this figure too, there is another local minimum, higher and situated near the edge of the Brillouin zone, in the [100] direction. In Fig. 3.1(a) the lowest conduction band minimum occurs near the zone edge. The band gap E_g is the energy difference between the minimum of E_c and the maximum of E_v and only in Fig 3.1 (b) they occur at the same **k**-value. Therefore, Fig 3.1 (b) represent a direct band gap semiconductor. Here an electron transferring from the top of the valence band to the bottom of the conduction band or vice versa changes only its energy and

not its momentum. In Fig 3.1(a), both energy and momentum simultaneously change thus representing an indirect band gap semiconductor.

The type of band is very important from the utilization point of view, since both energy and momentum conservation laws must hold during carrier generation or recombination. In an indirect semiconductor, the photon cannot account for the necessary momentum change in either generation or recombination. This means that other

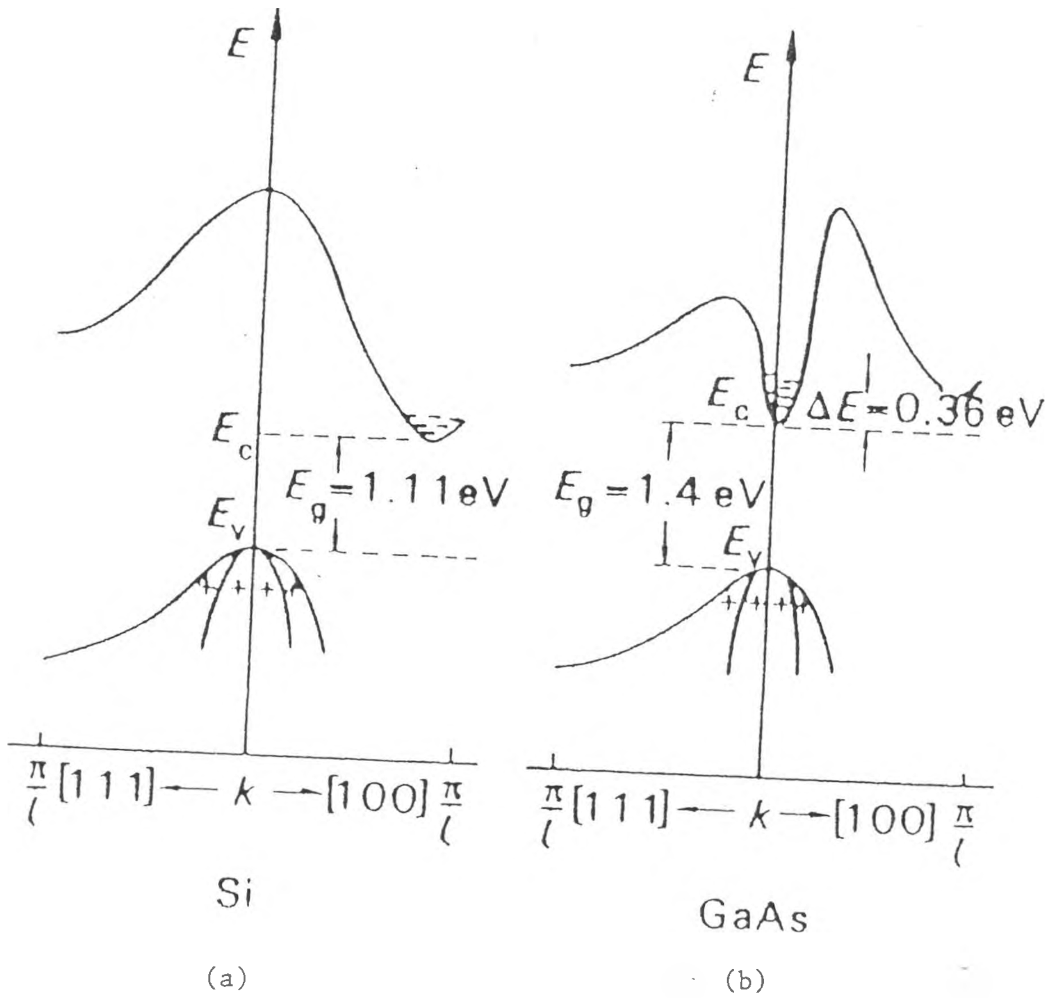

Fig. 3.1 : The energy bands in momentum space for (a) indirect band gap semiconductor (Si) and (b) direct band gap semiconductor (GaAs)

quantum particles, such as phonons, must participate and eitherremove or contribute the necessary excess momentum. This makesradiative recombination an unlikely process in indirect semiconductors. It is, a very likely process in direct band gap semiconductors. In an indirect semiconductor the most likely recombination process involves transfer of excess energy and momentum to several phonons, i.e. heating the lattice. The carrier is first trapped in a trapping centre, such as crystal defect, i.e., it becomes localized, gradually losing its energy and momentum photons until it finally recombines with an opposite carrier that passes by.

3.6 Electronic States

Transitions that occur between states within the conduction or valence band are known as intra-band transitions, whereas those that occur between states in different bands are called inter-band transitions. In any transition, energy is conserved. In crystalline semiconductors, long-range order imposes the additional rule of conservation of wave vector.

If $\mathbf{k}_i$ and $\mathbf{k}_f$ are the initial and final electron states wave vectors and $\mathbf{k}$ that of the light, then the conservation laws that apply are the following [34]

$$E_f - E_i = h\nu/2\pi$$

$$\mathbf{k}_i - \mathbf{k}_f = \mathbf{k} \qquad (3.9)$$

when $\mathbf{k}_i = \mathbf{k}_f$; $\mathbf{k} = 0$ implying that the optical transitions are essentially vertical on an electron E-**k** diagram.

In some interactions, this relation is not obeyed and this means that, in order to conserve wave vector, a third excitation must be involved. This is usually a phonon. In this case the relevant conservation laws are the following [34]

$$E_f - E_i = h(\nu - \nu_n)/2\pi$$

$$\mathbf{k}_f - \mathbf{k}_i = \mathbf{k} + \mathbf{K} \qquad (3.10)$$

where E_f and E_i are the final and initial energy of the electron state. ν and ν_n are the frequencies of the photon and phonon respectively.

3.7 Fundamental Electronic Absorption

Fig 3.2(a) is applicable to semiconductors such as GaAs [34], the minimum of conduction band occurs at the same **k**-value as the maximum of the valence band. This is known as a direct band gap. In this case, the absorption of a photon of energy equal to that of the minimum energy gap $h\nu/2\pi = E_g$ will give rise to a vertical transition on the energy band diagram, obeying the wave vector conservation law. Absorption (α) is very strong and expressed as [34]

$\alpha = A(h\nu/2\pi - E_g)^{1/2}$ (3.11)

where A is a constant. In materials such as Si (see Fig 3.2 (b)), the minimum of the conduction band and the maximum of the valence band do not occur at the same **k**-value [34]. This is an indirect band gap material. Hence, in order to maintain wave vector conservation during an optical transition, the process must be accompanied by the simultaneous absorption or emission of a phonon. Therefore, for indirect transition, absorption (α) is given by [34]

$$\alpha = C\left[\frac{(h(\upsilon-\upsilon_n)/2\pi - E_g)^2}{1-\exp(-h\upsilon_n/2\pi kT} + \frac{(h(\upsilon+\upsilon_n)/2\pi + E_g)^2}{\exp(-h\upsilon_n/2\pi kT)-1}\right] \quad (3.12)$$

where C is a constant. The first term of equation (3.12) represents photon absorption and so can only occur if $h\upsilon/2\pi > E_g - h\upsilon/2\pi$. The exponential term is the density of phonons available for absorption. The second term represents phonon emission and can only occur if $h\upsilon/2\pi > E_g + h\upsilon/2\pi$.

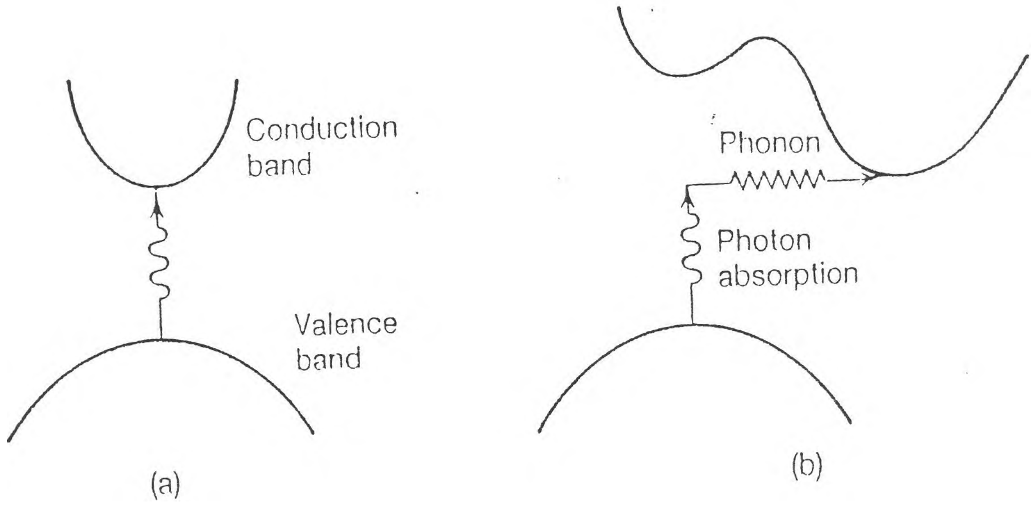

Fig. 3.2 : (a) shows a direct band gap semiconductor, such as GaAs.
(b) shows an indirect band gap semiconductor, such as Si.

3.8 Transmission and Reflection

Transmission (T_o) is given by the expression [22]

$$T_o = \frac{(1-R)^2 \exp(-\alpha t)}{1-R^2 \exp(-2\alpha t)} \qquad (3.13)$$

where R is reflectivity, t is film thickness and α is the absorption coefficient. When reflection is neglected equation (3.13) becomes

$$T = \exp(-\alpha t) \qquad (3.14)$$

The absorption coefficient can be determined using equation (3.14).

The reflectivity R at an absorbing medium of indices (n_r, k) in air for normal incidence is given by [10]

$$R = \frac{(n_r - 1)^2 + k^2}{(n_r + 1)^2 + k^2} \qquad (3.15)$$

where n_r is refractive index and k is the extinction coefficient. The absorption coefficient (α) is related to the extinction coefficient (k) by the expression [10]

$$k = \alpha\lambda / 4\pi \qquad (3.16)$$

where λ is the wavelength.

3.9 Figure of Merit for Transparent Conductors

The choice of a particular material is, in general, based on a set of performance requirement; these include electrical, optical, and mechanical properties as well as chemical stability. Moreover, raw material availability will have to be considered if large-scale deployment is anticipated.

Common to all transparent conductor applications is the need for optimizing the electrical and optical coating parameters. Depending on the type of device requiring a transparent electrode, the optical transmission and the electrical conduction of the electrode will have to exceed certain minimum values. Ideally, both parameters should be as large as possible. Their interrelationship, exclude, in most cases, the simultaneous achievement of maximum transmission and conduction.

The optical and electrical properties of a transparent conductor coating are best characterized by the electrical sheet resistance (R_s) and optical transmission (T_o). The sheet resistance is defined by [26]

$$R_s = 1/\sigma t \qquad (3.17)$$

where σ is the electrical conductivity and t is the coating thickness. The optical transmission (T_o) is given by [26]

$$T_0 = \exp(-\alpha t) \qquad (3.18)$$

where α is the optical absorption coefficient and t is thickness. A balance between transmission and sheet resistance can be achieved when the figure of merit (ϕ_{TC}) is defined as [26]

$$\phi_{TC} = T_0^{x}/R_s \qquad (3.19)$$

where x = 10 in order to simplify numerical calculations of practical figure of merit.

CHAPTER FOUR

4.0 EXPERIMENTAL TECHNIQUES

4.1 Introduction

Spray pyrolysis technique is normally used to prepare transparent and conducting thin films. In the case of Zn_2SnO_4, an alcoholic solution of zinc and tin salts is first atomized to fine droplets. The droplets are then transported to the hot substrate where they undergo a suitable reaction to form zinc stannate film. Several routes have been attempted in the past to obtain films with high optical transmittance, low resistivity, and good uniformity, using widely differing spray set ups, spray mixtures, and spray methods. One of the major limitations of the spray deposition technique is its low efficiency of film growth. In spray pyrolysis, better growth rate is realized when the droplets are transported to the substrate in an ideal fashion, i.e. as the droplets approach the surface, the solvent in the droplet vaporizes completely. The droplets undergo vaporization if their residence time in the vicinity of hot substrate surface is sufficiently long so as to warm it up to the ambient temperature while simultaneously retaining appropriate size. The time available for the warm up in the vicinity of the substrate depends upon the droplets velocity, which in turn depends on the propelling and retarding forces acting on them. In many experimental situations, the control on the retarding forces operating on the droplets is limited, which seriously restrict the frequency at which the droplets are transported to the

substrate and thus the growth rate. The optimum velocity for the droplets is often obtained by adjusting the control parameters such as solution and gas flow rates, substrate-to-nozzle distance e.t.c.

In many practical systems, the flow conditions are adjusted such that the droplets and the air move with nearly same velocity near the substrate. The dominant forces acting on such droplets are forces due to gravity, Stoke's force, and a thermophoretic force. The Stoke's force is given by [9]

$$F_s = -6\pi\eta_a r (V_d - V_a) \qquad (4.1)$$

where V_d and V_a are the velocities of the droplet and air respectively, η_a is the viscosity of the air and r is the radius of the droplet.

The thermophoretic force (F_t) is given by [9]

$$F_t = \frac{-9\pi K_a \eta_a r \rho_a T_a}{(2K_a + K_d)\Delta T} \qquad (4.2)$$

where K_a and K_d are the thermal conductivities of the air and the aerosol droplet respectively, η_a is the viscosity of the air, ρ_a is the density of the air and ΔT_a is the thermal gradient of the air. As the droplet velocity and air velocity are nearly the same, the Stoke's force is negligibly small. As the droplet size

is small, the gravity force is also negligible. Thus in most experimental situation, the time spent by the droplet in the vicinity of the substrate appears to be governed by the retarding thermophoretic force.

The Stoke's force acting on the droplets can provide the desired temporal variation in the retarding force under appropriate conditions. If the droplets are launched at a velocity "V_o" into the "still" air, a large Stoke's force proportional to the relative velocity, retards their motion thereby reducing their velocity continuously with time. Under this force, the droplets come to a halt at a distance, known as stop distance, after a relaxation time "t" characteristic of the drop size. For the motion governed by the stoke's law of resistance, the relaxation time (τ) is given by [9]

$$t = m/6\pi\eta_a r \qquad (4.3)$$

where m is the mass of the droplet, r its radius, and η_a the viscosity of the air and the stop distance is given by $\mathbf{d = tV_o}$. The motion of the droplets thereafter is governed by gravity and moves with a velocity $V_s = gt$. Within this stop distance the droplets are subject to different magnitudes of retarding forces and thus possess different velocities. By appropriate choice of starting velocity and substrate-to-nozzle distance, the droplet residence time in the vicinity of the substrate can be closely controlled. Transparent conducting zinc stannate films were

prepared by adjusting the deposition conditions so as to favour faster growth.

4.2 Experimental Set-Up

The experimental set-up of the spray pyrolysis system used is shown in the Fig. 4.1. The sprayer made of glass, had two inlets, one for the solution, while the other was for the gas, and a single outlet. To obtain a fine spray the outlet was a fine capillary. Oxygen was used as a carrier gas. Glass slides (2.5 x 2.5 cm) were thoroughly cleaned using a detergent and then dipped in acetone to remove grease particles before finally rinsing with distilled water. Cleaned glass slides were dried in an Eyela Windy Oven WFD-1000ND. Clean dry glass slides (substrates) were placed on the thick cast iron metal and the electric heater switched on. The temperature of the substrate was monitored using a thermocouple thermometer.

4.2.1 Film growth

A mixture of two parts of (0.1 - 0.4)M solution of $ZnCl_2$ in isopropyl and water (volume ratio, 3:1) and one part of (0.1 - 0.4)M solution of $SnCl_4.5H_2O$ in butane-1-ol and water (volume ratio, 3:1) constituted the precursor solution. Trial spraying were carried out to determine the best gas pressure, spraying height and the temperature that gave the best film. With suitable height, gas pressure and temperature, the mixture was sprayed on the glass substrate for a few seconds and stopped to allow the temperature gain its optimum value i.e., during spraying the glass substrates were allowed a temperature variation of $\pm 5\ ^{\circ}C$

only. The glass substrates were held at temperatures ranging between 350 and 450 °C. The spray process was repeated till thin films formed on the substrate. Quick cooling of the film was done to avoid annealing effect by connecting the substrate support base (thick cast iron piece) to cold tap water via a conducting metal bar that created a high temperature gradient. Uniform film thickness was ensured through movement of the spray over the glass substrate slowly while spraying.

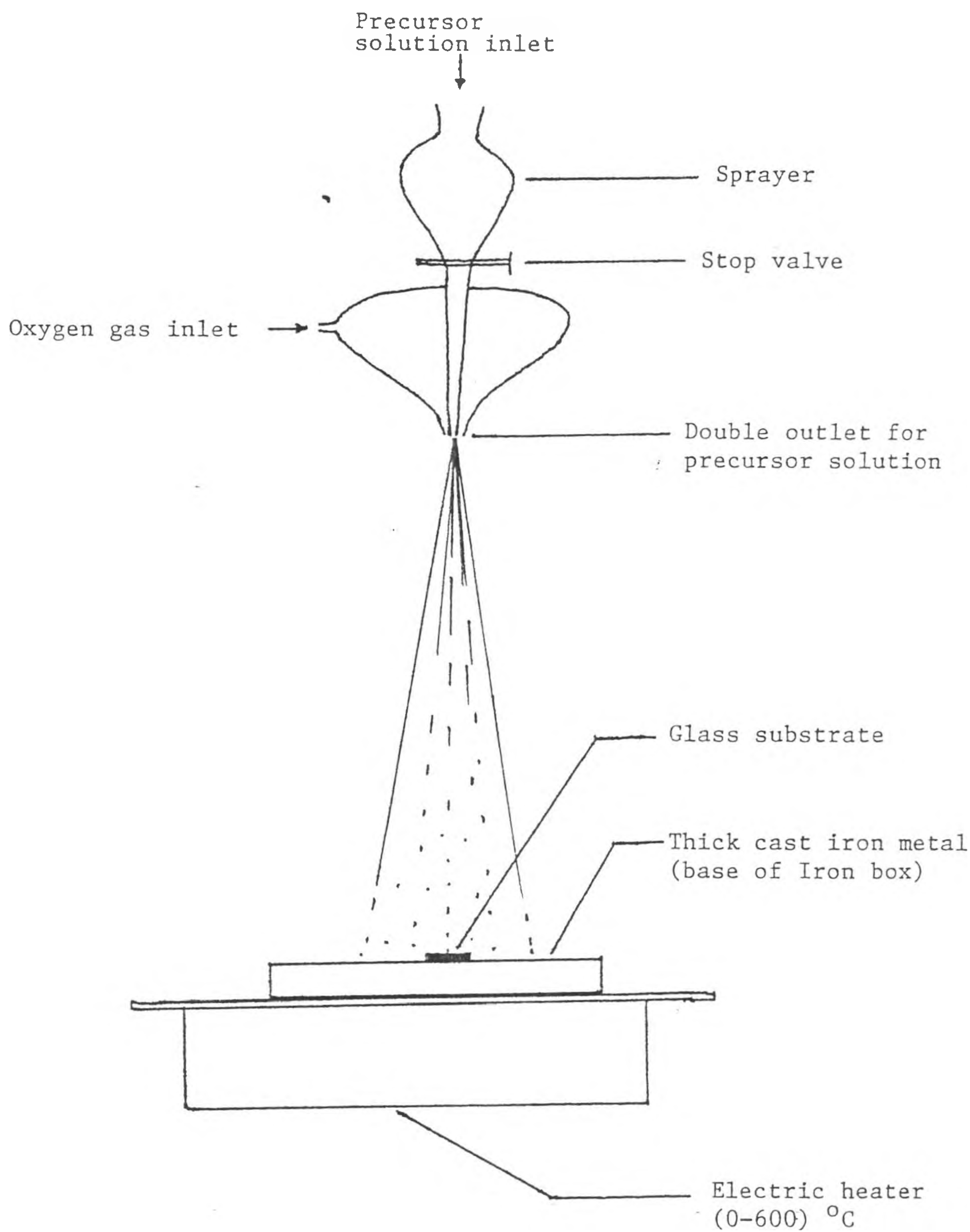

Fig. 4.1 : Experimental set-up for spray pyrolysis technique

4.3 Transmission and Sheet Resistance Measurements

The transmission of the light through the films was measured using a UV-120-02 Shimadzu spectrophotometer. The sheet resistance of the zinc stannate films was measured by the two probe method.

4.4 Annealing Studies

Annealing studies in vacuum and in air ambient were carried on the zinc stannate films heated using a radiant heater up to 120 °C and annealed for two hours. Air at atmospheric pressure and a vacuum of about 1.5×10^{-4} Torr respectively were the ambient conditions at which the studies were undertaken. The electrical resistivities of the films were monitored during the heating and the cooling cycles. The electrical (resistivity and mobility) and optical (absorption coefficient, extinction coefficient and band gap) properties of annealed films were studied.

4.5 Determination of Band Gap

The transmission ratio (T_{1-2}) for two films of different thickness was obtained directly by the ratio recording technique as [10]

$$T_{1-2} = \exp(-\alpha\Delta t) \qquad (4.4)$$

where Δt is the thickness difference of the two films and α is the absorption coefficient. The ratio of transmission was obtained by placing two films of different thickness, the thicker in the sample beam and the thinner in the reference beam, in a

UV-120-02 Shimadzu spectrophotometer in order to cancel out the reflection effects. For direct transitions, a plot of $(\alpha\Delta th\nu)^2$ against $h\nu$, where $h\nu$ is the incident energy, gives a straight line which on extrapolation cuts the energy axis at the band gap value [22].

4.6 Film thickness Measurement

Interference of rays reflected from two different planes can give rise to pronounced maxima and minima in intensity. When the path length through the sample corresponds to an integral number of wavelengths, constructive interference will occur, and for paths of an odd number of wavelengths, minima of intensity will occur hence leading to a relation between thickness t, and the wavelength λ, where a particular maximum or minimum occurs. Thus, using spectrophotometer chart showing fringes, thickness was calculated directly using the expression [23]

$$t = \frac{m\lambda_o\lambda_m}{2n(\lambda_o - \lambda_m)\cos\phi} \qquad (4.5)$$

where m is the number of maxima from λ_o to λ_m, λ_m is the wavelength at successive maxima, ϕ is the angle of incidence of the beam as it hits the lower reflecting surface and n is the refractive index. This method was used to determine the thickness of the zinc stannate films. It has an additional advantage of compensating for any phase-shift differences between the two

surfaces as long as they are independent of wavelength. This kind of measurement is widely used because it is nondestructive.

4.7 Hall Effect Studies

The Hall measurements were made for high and low resistivity films. The set-up was as shown in Fig. 4.2. The film was placed in a perpendicular magnetic field B_z. A current was passed through the film in the y-direction, creating an electric field in the x-direction. The current (I_y) was varied and the corresponding voltage (V_H) measured. The Hall coefficient R_H was computed using the formula [24]

$$R_H = E_x/J_yB_z \tag{4.6}$$

where B_z was measured using a fluxmeter. E_x was calculated from V_H/L and J_y was calculated from I_y/tL where t and L were the thickness and length of the film respectively. The carrier concentration and the mobility were determined from [24]

$$N = 1/R_Hq \quad \text{and} \quad m_H = R_Hs \tag{4.7}$$

respectively.

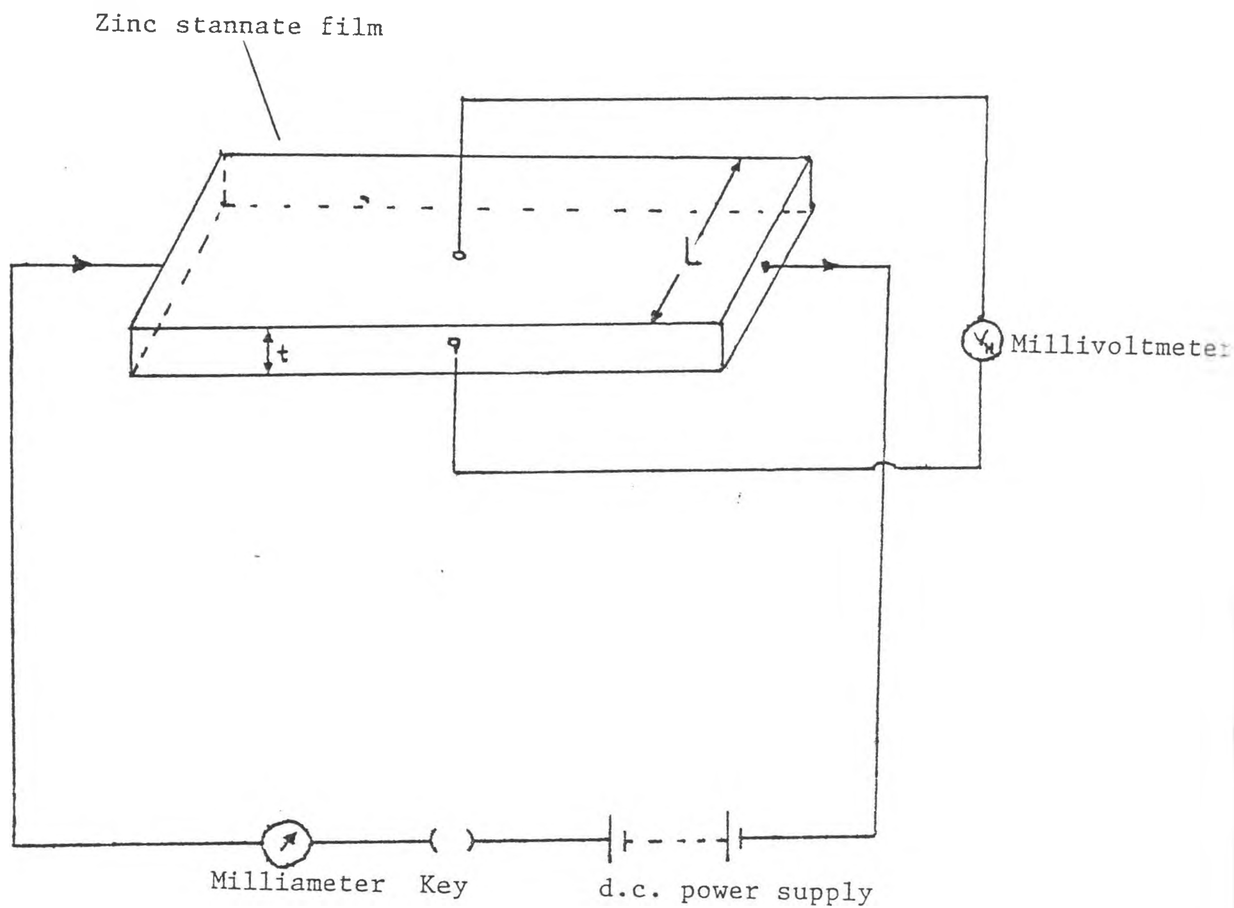

Fig. 4.2 : Hall effect measurements set-up

4.8 Structural and Topographic Studies

The structure of the films was studied using an automated Phillips (PM 9920/05) x-ray diffractometer by observing the effect of deposition parameters and annealing on the crystallinity of the films. Whereas the surface topography studies were done using a JSM -T100 (JEOL) scanning electron microscope.

CHAPTER FIVE

RESULTS AND DISCUSSION

5.1 Optimization of Growth Parameters

The growth parameters optimized were pressure, spray height, spray rate and substrate temperature. Each parameter was studied separately i.e. varied while the rest were kept constant. For each parameter the one that gave the best film growth with the best optical and electrical properties was selected. A gas pressure of approximately 7.5×10^4 Nm^{-2}, spray height of 30 cm and a spray rate of 15 cm^3 per minute were selected as optimum parameters. For low spray height, the substrate cracked due to rapid cooling, while for heights above 30 cm, a lot of solution was wasted and the resulting film had a very high resistivity due to prolonged annealing of film in the air that enhanced chemisorption process. For higher spray rates, the resistance was very high (> 20 MΩ) and the optical properties of the films were poor, since white spots were evident. The white spots resulted from big droplets which on reaching the substrate surface could not decompose immediately, but rather slowly leaving a white precipitate.

For very low spray rates the sheet resistance was very high (> 20 MΩ/□). The high resistivity for both low spray rate and high height sprayed Zn_2SnO_4 films can be attributed to annealing effects since it took longer time to grow the film under these

conditions. Whereas for substrate temperature, a temperature of 440 °C was taken as the optimum substrate temperature for depositing Zn_2SnO_4 thin films. Fig. 5.1 shows the variation of sheet resistance with substrate temperature. It shows a drop in sheet resistance as temperature rises and after a minimum it increases again. Sheet resistance was high for both substrate temperature lower and higher than 440 °C. This could be due to incomplete reaction at lower substrate temperature and cracked films at higher substrate temperatures. Overheating of the substrate causes a negative influence on the crystallographic properties, for instance, in the case of ZnO films [5], the lattice constants and grain sizes reversed direction of variation with temperature at optimum substrate temperature. On the other hand, grain size increased with substrate temperature except, beyond optimum temperature where it reduced as substrate temperature increased. It can be seen that the largest grain size was obtained at 440°C substrate temperature (see Fig. 5.2). Hence these films had the lowest sheet resistance [8].

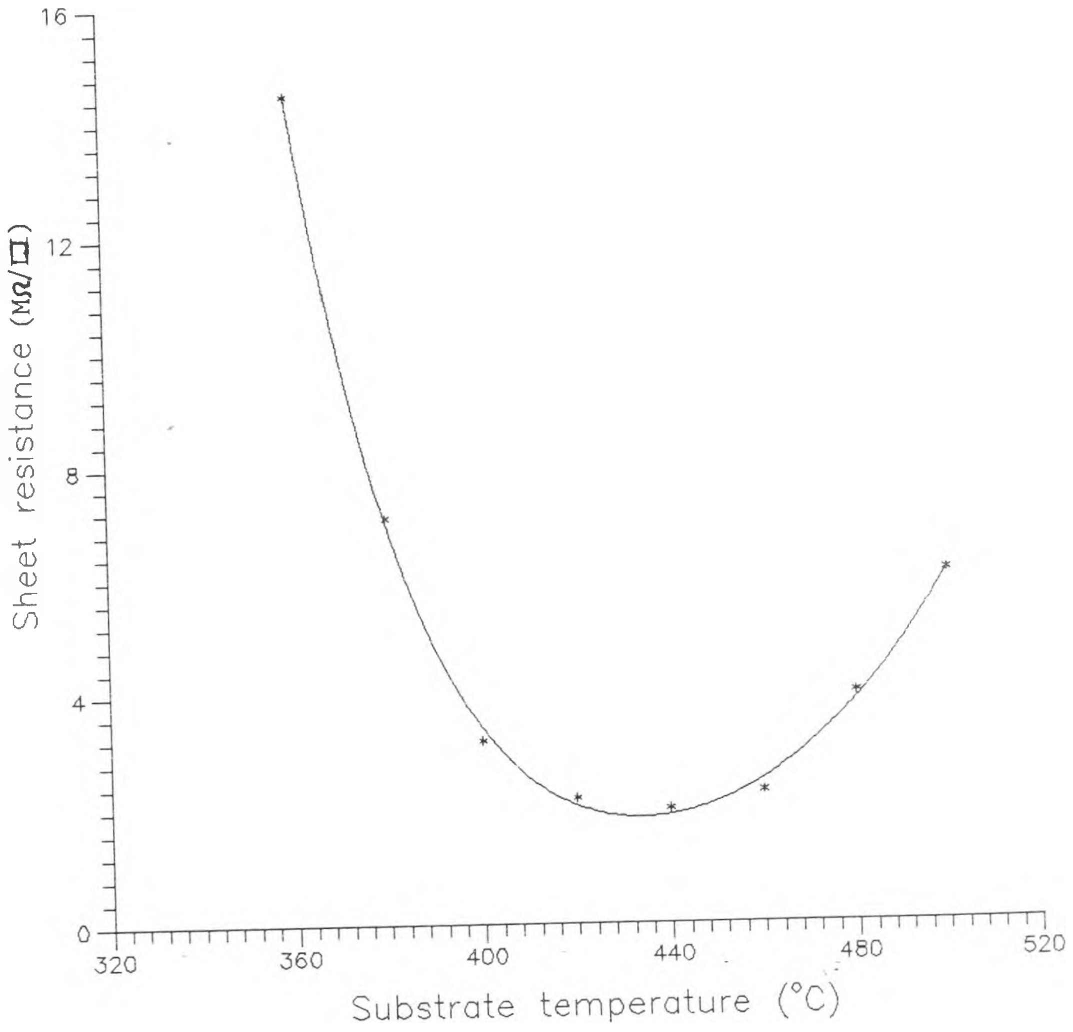

Fig. 5.1 : Variation of sheet resistance with substrate temperature

5.2 Structural Properties Of Zn_2SnO_4 Films

5.2.1 Surface Topography

Surface topography of Zn_2SnO_4 films is shown in the scanning electron micrographs (see Fig. 5.2) for two different substrate temperatures 380 °C and 440 °C, respectively. Films grown at 440 °C had bigger grain sizes than those grown at 380 °C. Shanthi *et al* [8] recorded similar observation for undoped tin oxide films. Better crystallinity of films grown at 440 °C is confirmed by X-ray diffraction pattern (see Fig. 5.3).

5.2.2 X-Ray Diffraction Studies

The substrate temperature dependence of the X-ray diffraction pattern of the (002) peak is shown in Fig. 5.3. Zn_2SnO_4 films grown at 380 °C were highly amorphous and their X-ray diffraction pattern is shown in Fig. 5.3(a). Fig. 5.3(b) shows a peak observed for Zn_2SnO_4 (002) plane, indicating a strong c-axis normal to the substrate surface. Only (002) diffraction peaks of Zn_2SnO_4 were observed. This kind of pattern was observed for Zn_2SnO_4 films with substrate temperature of 400 °C. The peak shown in Fig. 5.3 (b) is positioned at 34.5° diffraction angle which corresponds to the Zn_2SnO_4 (002) peak given in the Inorganic Phases (1980) Powder Diffraction File [25]. All films grown at 380 °C and below exhibited the X-ray diffraction pattern shown in Fig. 5.3 (a). Whereas those grown

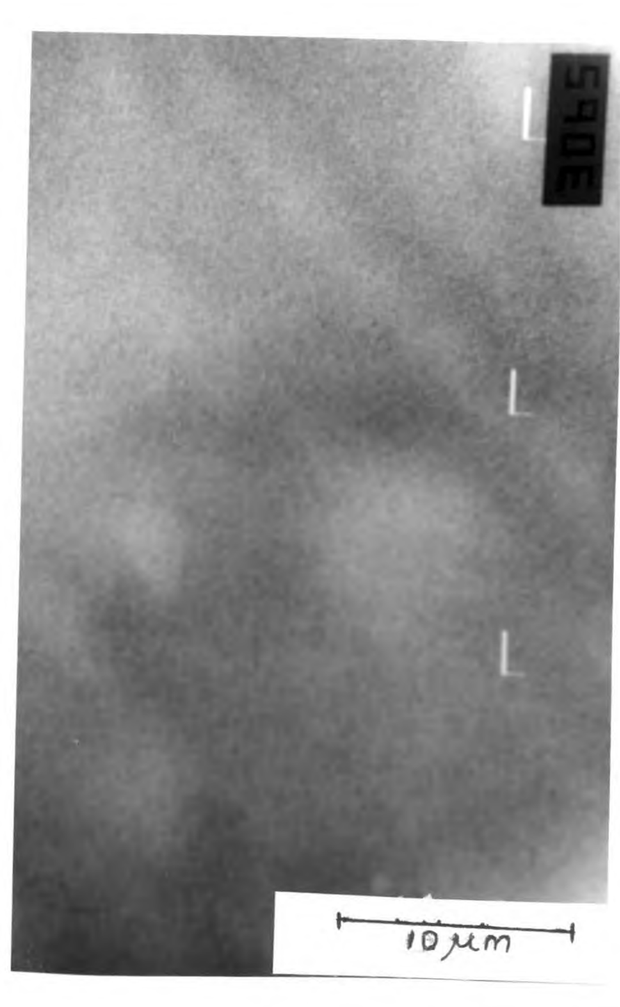

(a)

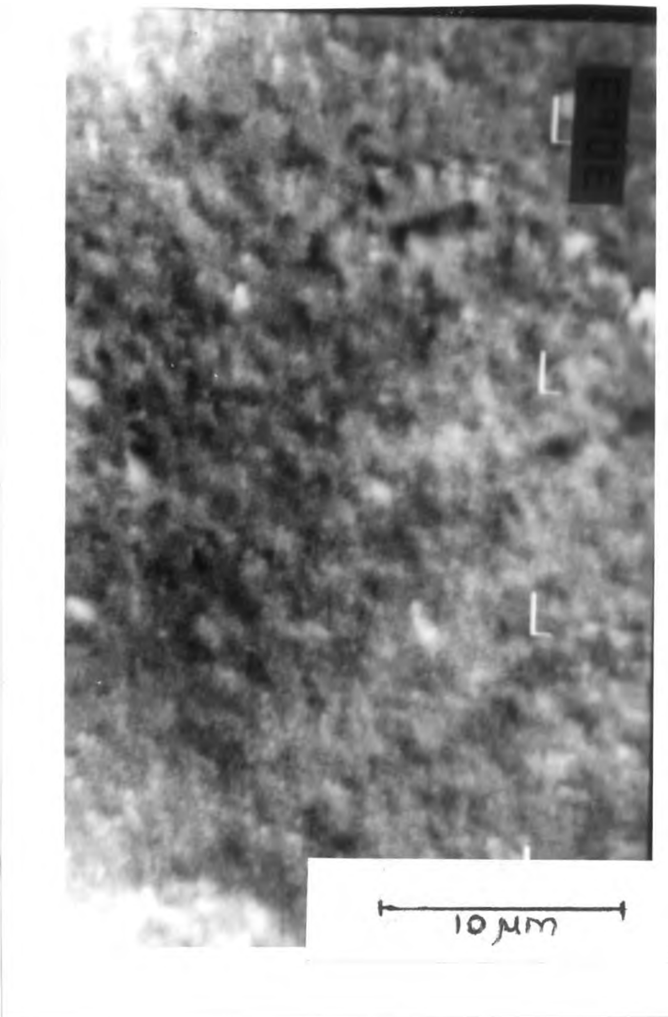

(b)

Fig. 5.2 : Scanning electron micrographs of vacuum annealed films films with substrate temperature of (a) 380 °C and (b) 440 °C.

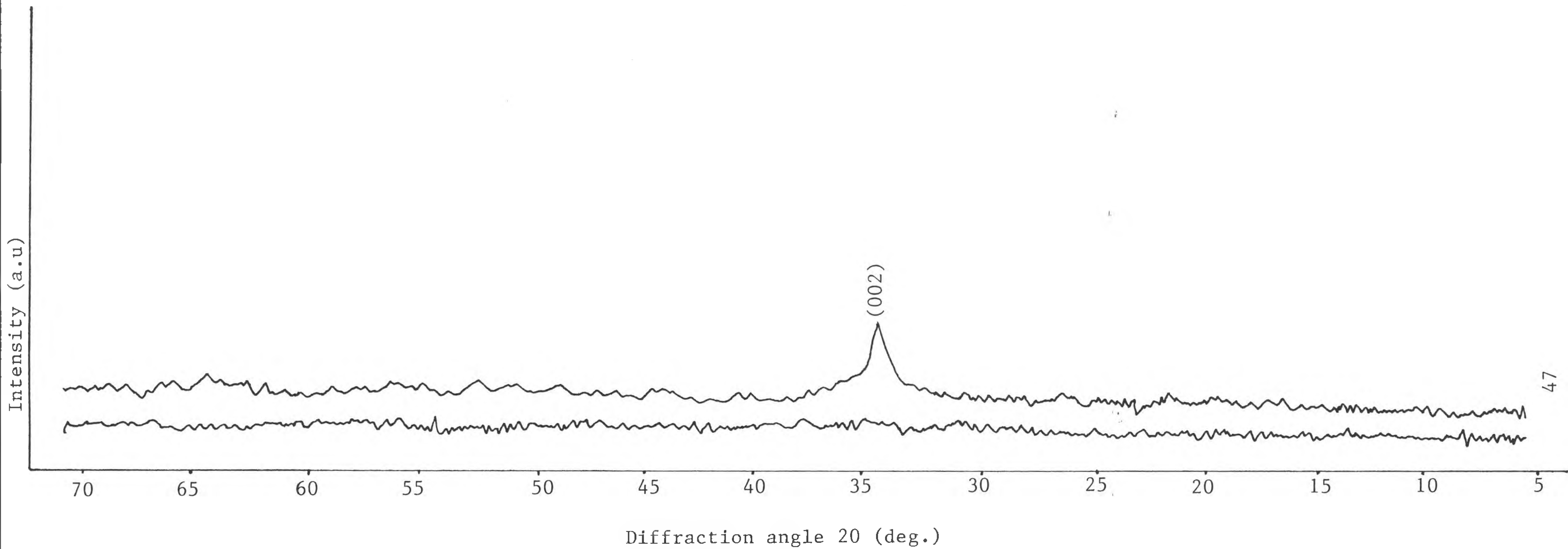

Fig. 5.3 : X-ray diffraction pattern for zinc stannate films grown at (a) 380 °C (b) 440 °C.

at substrate temperatures above 380 °C exhibited the X-ray diffraction pattern shown in Fig. 5.3 (b).

5.3 Optical Properties.

5.3.1 Transmission Spectra

Fig. 5.4 shows the transmission spectra for zinc stannate films grown at different substrate temperatures. The transmission decreased with increase in substrate temperature. As substrate temperature increased, better growth and crystallization of Zn_2SnO_4 films was achieved which concurrently led to an increase in carrier concentration. The increase in carrier concentration reduced transmission by increasing reflectivity.

Fig. 5.5 shows the transmission spectra for Zn_2SnO_4 films before and after annealing at 100 °C in vacuum (1.5×10^{-4} Torr). Carrier concentration increased on annealing in vacuum. The increase in carrier concentration was attributed to an increase in number of oxygen vacancies. The increase in carrier concentration increased reflectivity; consequently, reducing transmission.

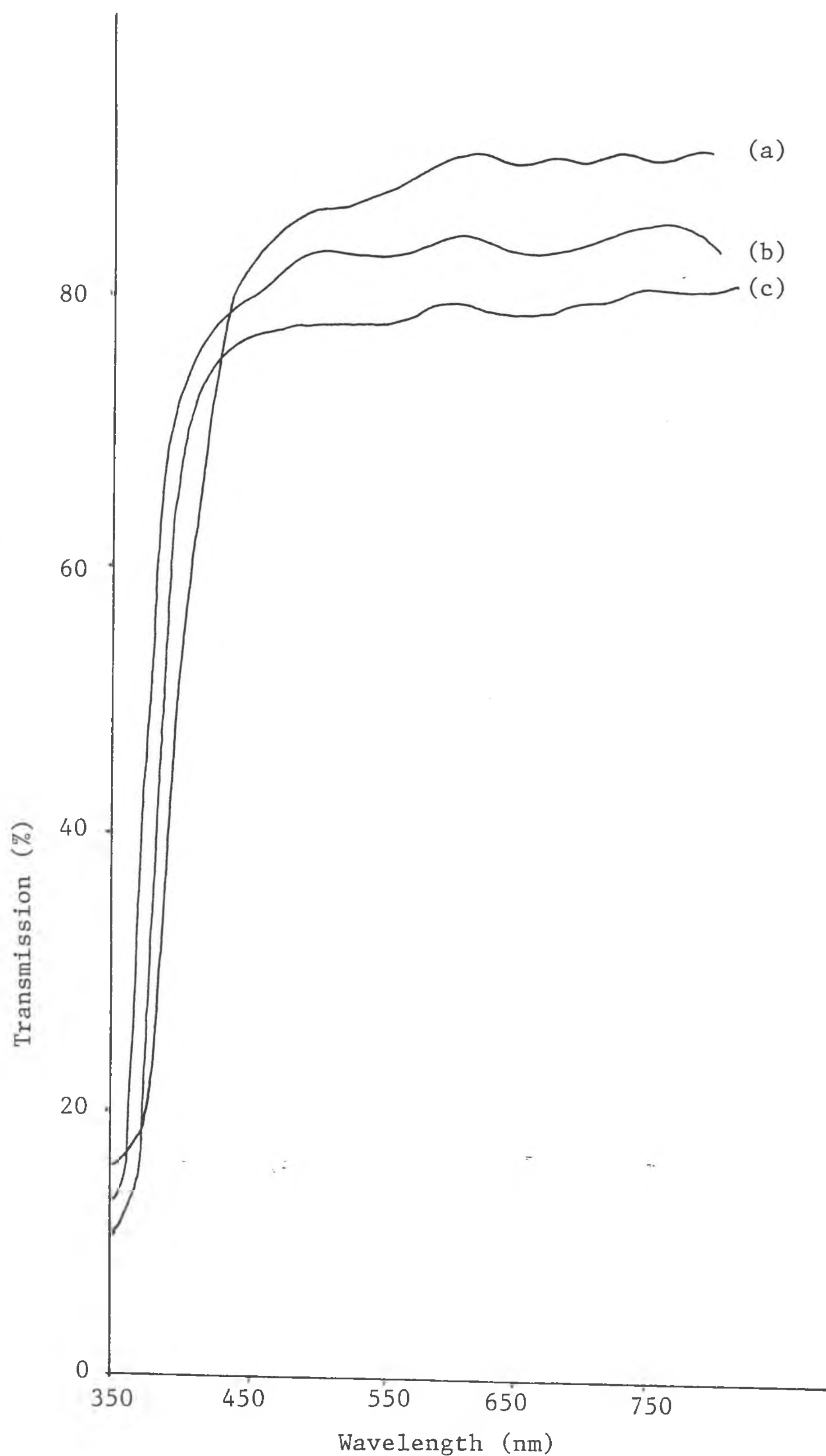

Fig. 5.4 : Transmission spectra for zinc stannate films grown at (a) 350 °C, (b) 400 °C and (c) 440 °C.

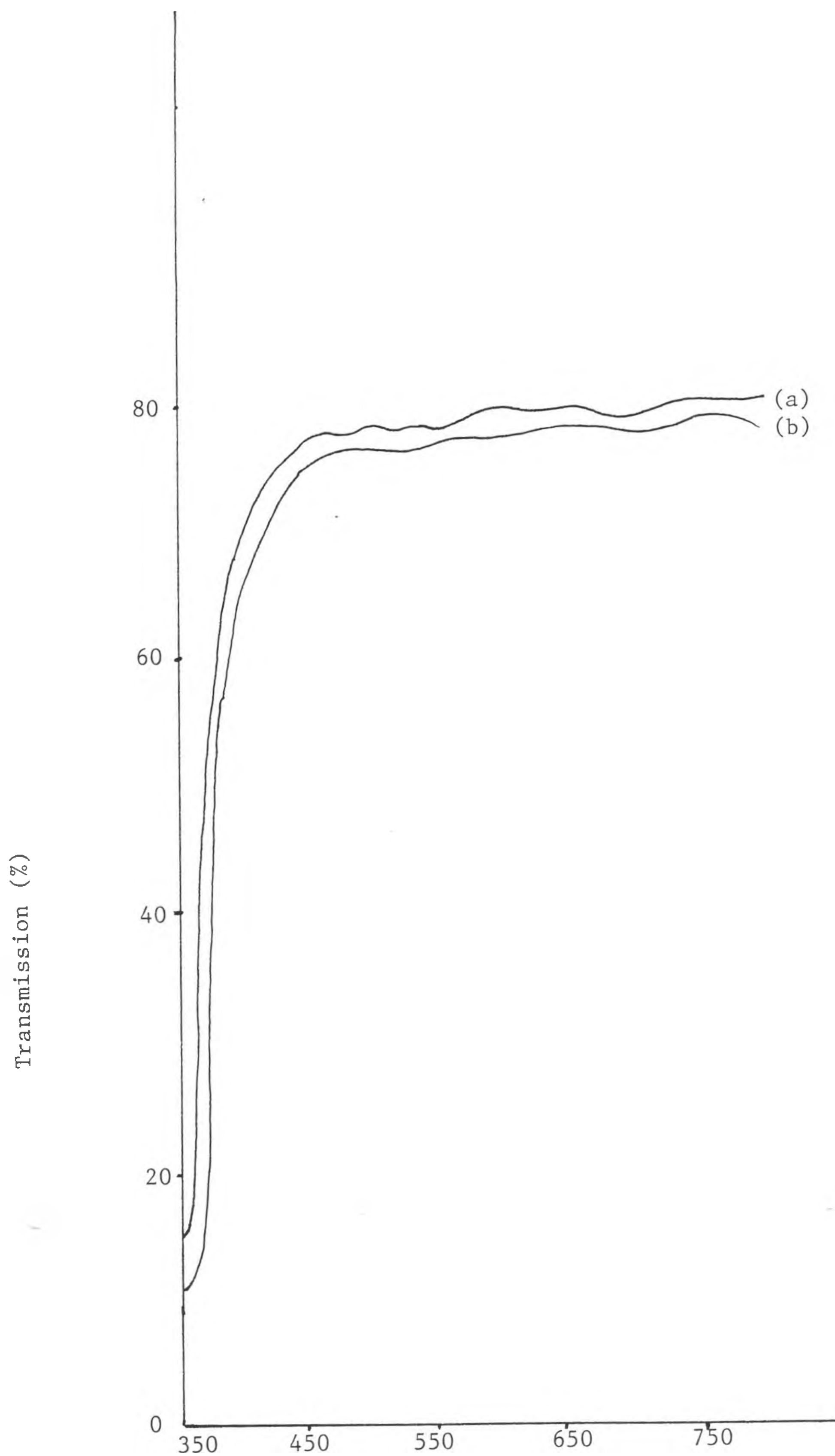

Fig. 5.5 : Transmission spectra for (a) as-deposited zinc stannate films and (b) after annealing in vacuum.

5.3.2 Absorption Coefficient

Absorption coefficient α, was calculated using thickness t, that was obtained by optical method. The optical method employs interference fringes obtained on spectrophotometer charts. Fig. 5.6 shows interference fringes from which the thickness was calculated (see appendix A) directly using the expression [23]

$$t = m\lambda_o\lambda_m/2n_r(\lambda_m-\lambda_o)\cos\phi \qquad (5.1)$$

The absorption coefficient was computed using transmission data (see appendix B) and the equation [10]

$$T_o = \exp(-\alpha t) \qquad (5.2)$$

where reflection was neglected. The results were tabulated in Table 1. Fig. 5.7 shows variation of absorption coefficient with wavelength. Using this figure we can deduce that the optical band edge for Zn_2SnO_4 films lies around 400 nm wavelength. This is because for wavelengths below 400 nm, the absorption coefficient is very high and appear to increase as wavelength decreases leading to almost total absorption of incident light. Whereas for wavelengths above 400 nm, the transmission is over 50% and quickly approaches 80% with a steady absorption coefficient that justifies Zn_2SnO_4 to be

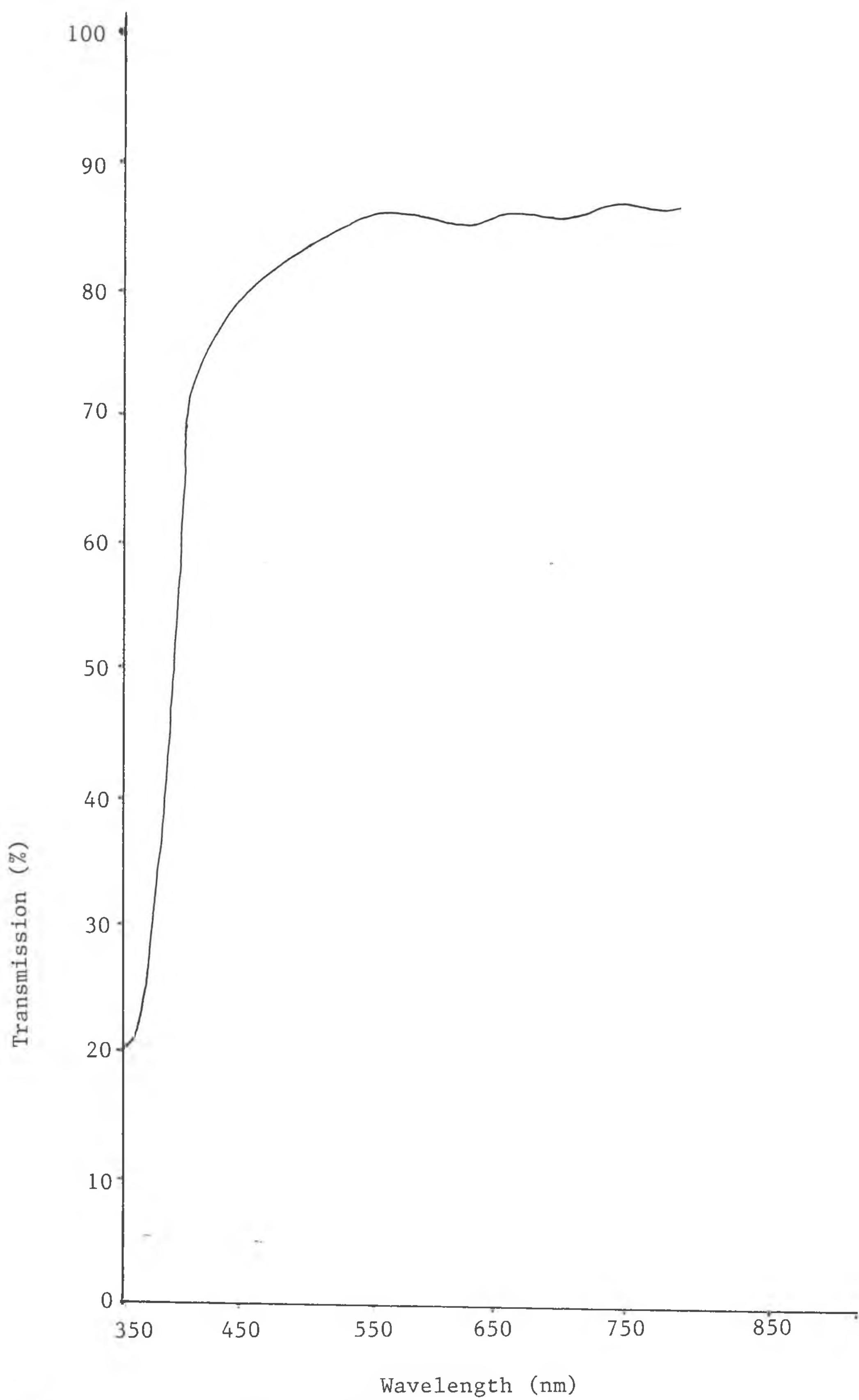

Fig. 5.6 : Interference fringes

classified as a transparent material in this region of the spectra.

Table 1 : Values of transmission (T_o), wavelength (λ), absorption coefficient (α) and photon energy ($h\nu$) for Zn_2SnO_4 film of thickness 1592.6 A

T_o	λ (nm)	$\alpha (10^5 cm^{-1})$	$h\nu (eV)$
0.022	350	2.4	3.547
0.097	370	1.47	3.355
0.216	390	0.96	3.183
0.605	410	0.32	3.028
0.695	430	0.23	2.889
0.732	450	0.20	2.760
0.754	470	0.18	2.643
0.766	490	0.17	2.535
0.786	510	0.15	2.436
0.799	530	0.14	2.344

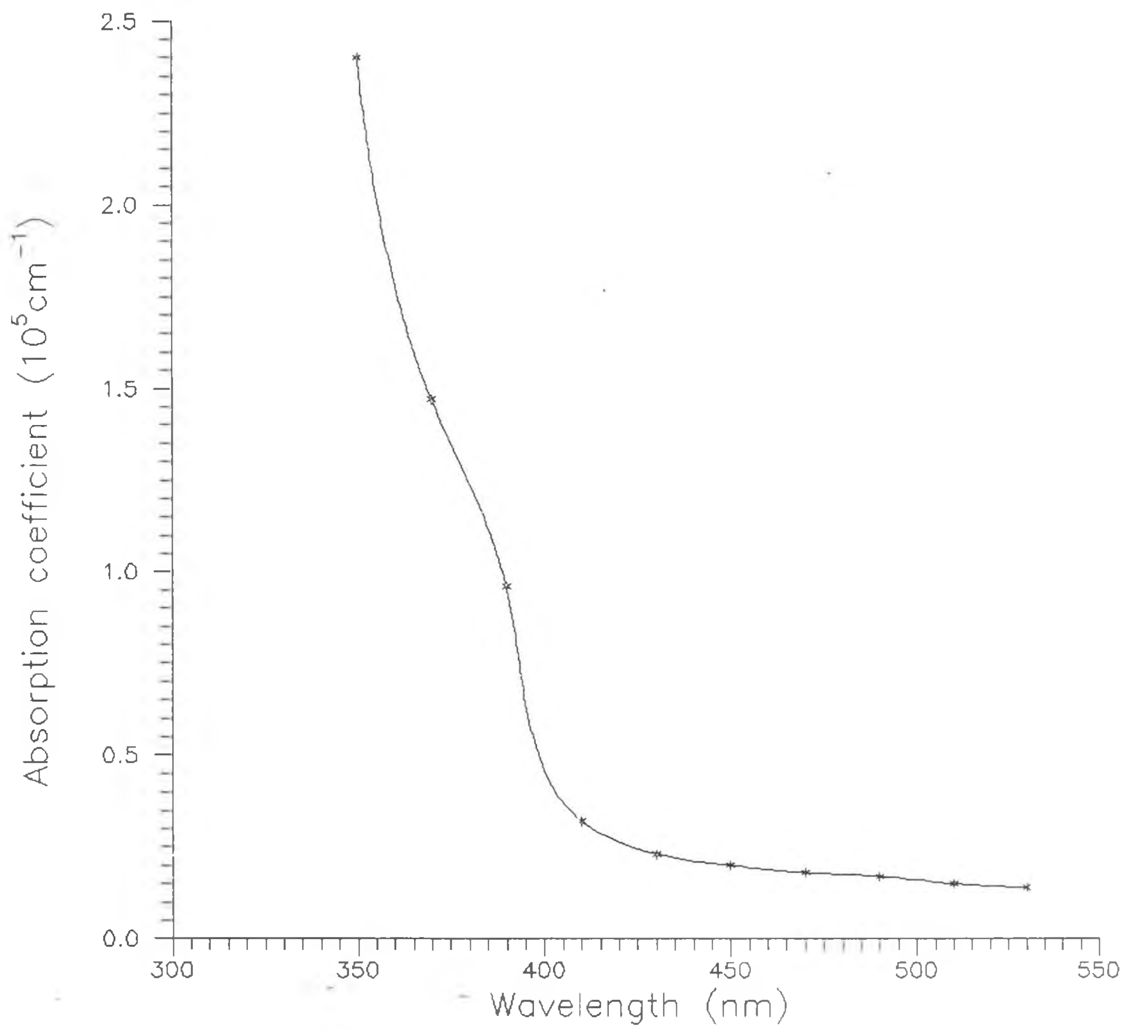

Fig. 5.7 : Absorption coefficient Vs. wavelength

5.3.3 Extinction Coefficient

Parameters comprising of real and imaginary parts, characterize the optical properties of a medium. The real part generally gives an idea about dispersion, while the imaginary part provides a measure of dissipation rate of the wave in the medium. one of these parameters is the index of refraction [10].

$$N = n - ik \qquad (5.3)$$

where n is the ordinary index and k is the extinction coefficient. The extinction coefficient is given by [10]

$$k = \alpha l/4\pi \qquad (5.4)$$

where λ is the wavelength and α is the absorption coefficient. Using this expression and Table 1, Table 2 was tabulated. Fig. 5.8 shows variation of extinction coefficient with photon energy. It is observed that for photon energy less than 3 eV (i.e. for wavelength greater than 410 nm) the extinction coefficient is minimum and approximately constant. This observation reinforces the classification of Zn_2SnO_4 as a transparent material in the (410-1000)nm range of the spectra.

Table 2. : Values of wavelength (λ), extinction coefficient (k) and photon energy ($h\nu$) for Zn_2SnO_4 films of thickness 1592.6 A and refractive index 2.

λ(nm)	k x 10^{-1}	$h\nu$ (eV)
350	6.67	3.549
370	4.31	3.355
390	2.98	3.183
410	1.03	3.028
430	0.78	2.889
450	0.70	2.760
470	0.66	2.643
490	0.65	2.535
510	0.61	2.436
530	0.59	2.344

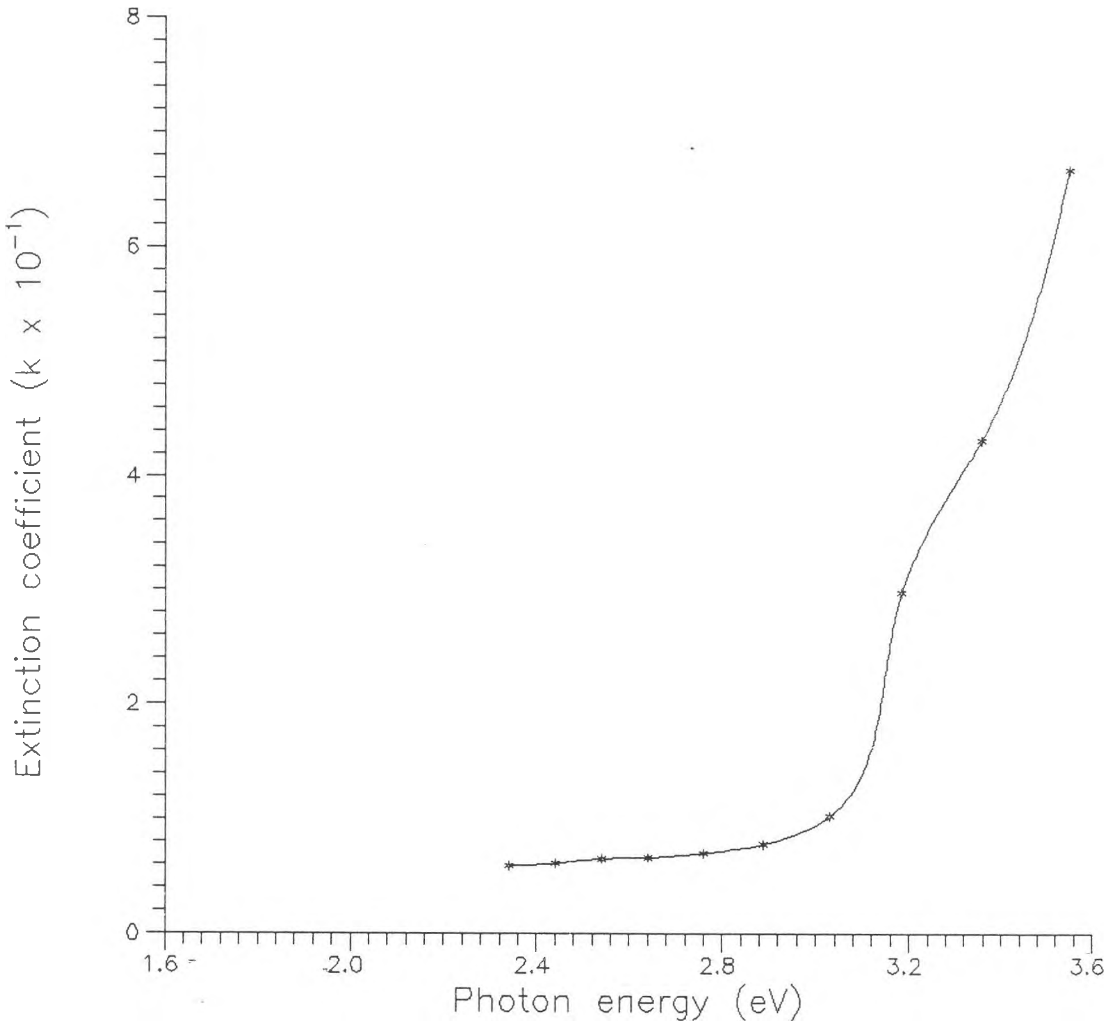

Fig. 5.8 : Extinction coefficient Vs. photon energy

5.3.4 : Band Gap

A ratio recording technique was used to determine the band gap of Zn_2SnO_4 films using two films of different thickness. The films were deposited at optimum conditions except for the duration of coating. Fig. 5.9 shows the transmission spectrum of a thicker film relative to a thinner film of Zn_2SnO_4. From this figure, Table 3 was tabulated. The energy band gap was obtained by extrapolating the linear portion of the plot of $(\alpha\Delta th\nu)^2$ against $h\nu$ to $(\alpha\Delta th\nu)^2 = 0$ (see Fig 5.10). The band gap was found to be approximately 3.1 eV. Therefore Zn_2SnO_4 is a wide band gap transparent semiconductor hence transparent to solar radiation and can be used as windows when deposited onto silicon. Similar observations have been reported on SnO_2 films by Shanthi *et al* [8] and Abass *et al* [10].

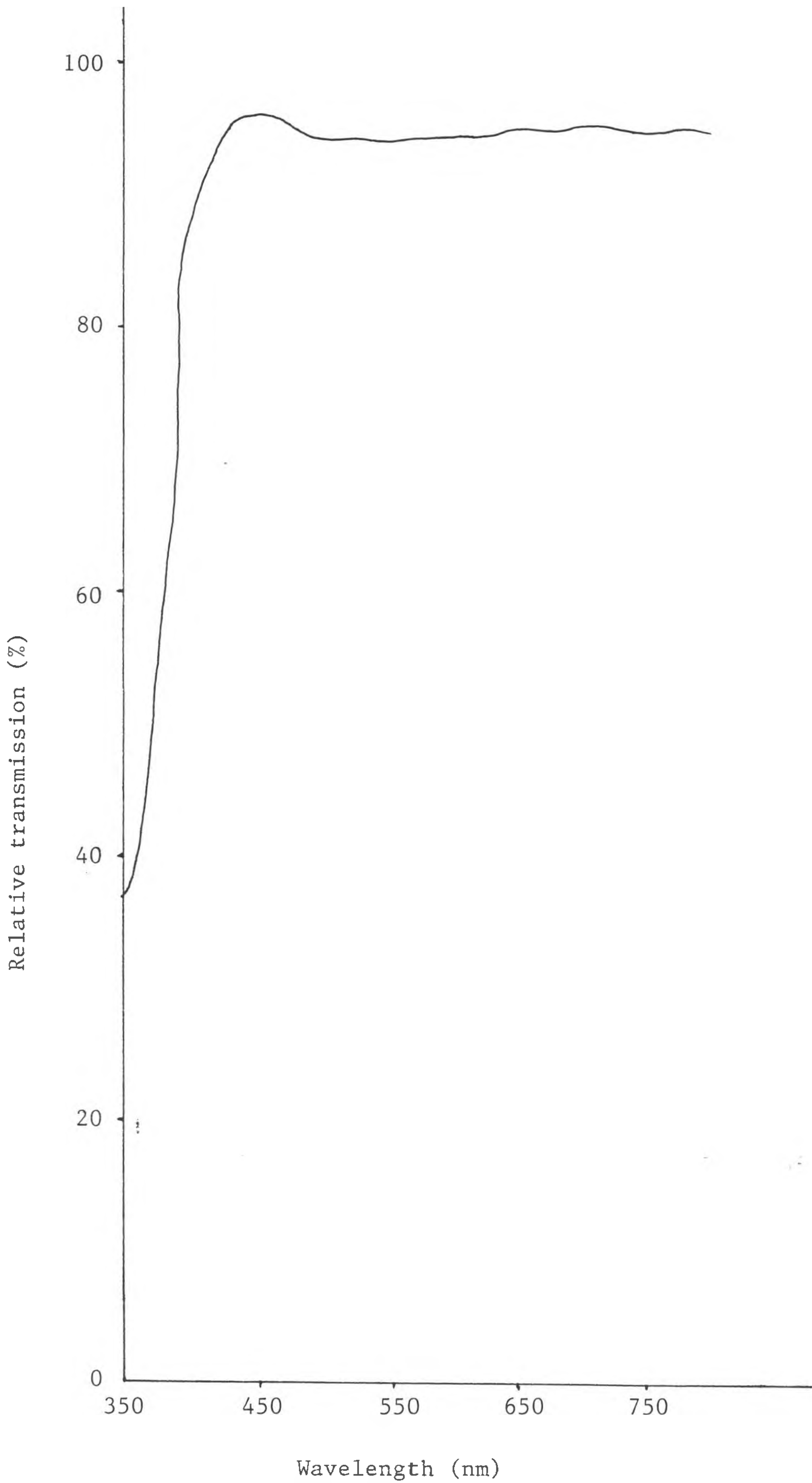

Fig. 5.9 : Transmission spectrum of a thicker film relative to a thinner zinc stannate film.

Table 3. Values of relative transmission (T_{1-2}), wavelength (λ), photon energy ($h\nu$), $\alpha\Delta t$ and $(h\nu\alpha\Delta t)^2$ used to determine band gap.

T_{1-2}	λ (nm)	$(h\nu\alpha\Delta t)^2$ $(eV)^2$	$h\nu$ (eV)	$-In(T_{1-2}) = \alpha\Delta t$
0.36	350	13.141	3.547	1.022
0.41	360	9.459	3.448	0.892
0.45	370	7.168	3.355	0.798
0.48	380	5.750	3.267	0.734
0.63	390	2.162	3.183	0.462
0.88	400	0.158	3.103	0.128
0.97	410	0.008	3.028	0.03
0.98	420	0.003	2.956	0.02

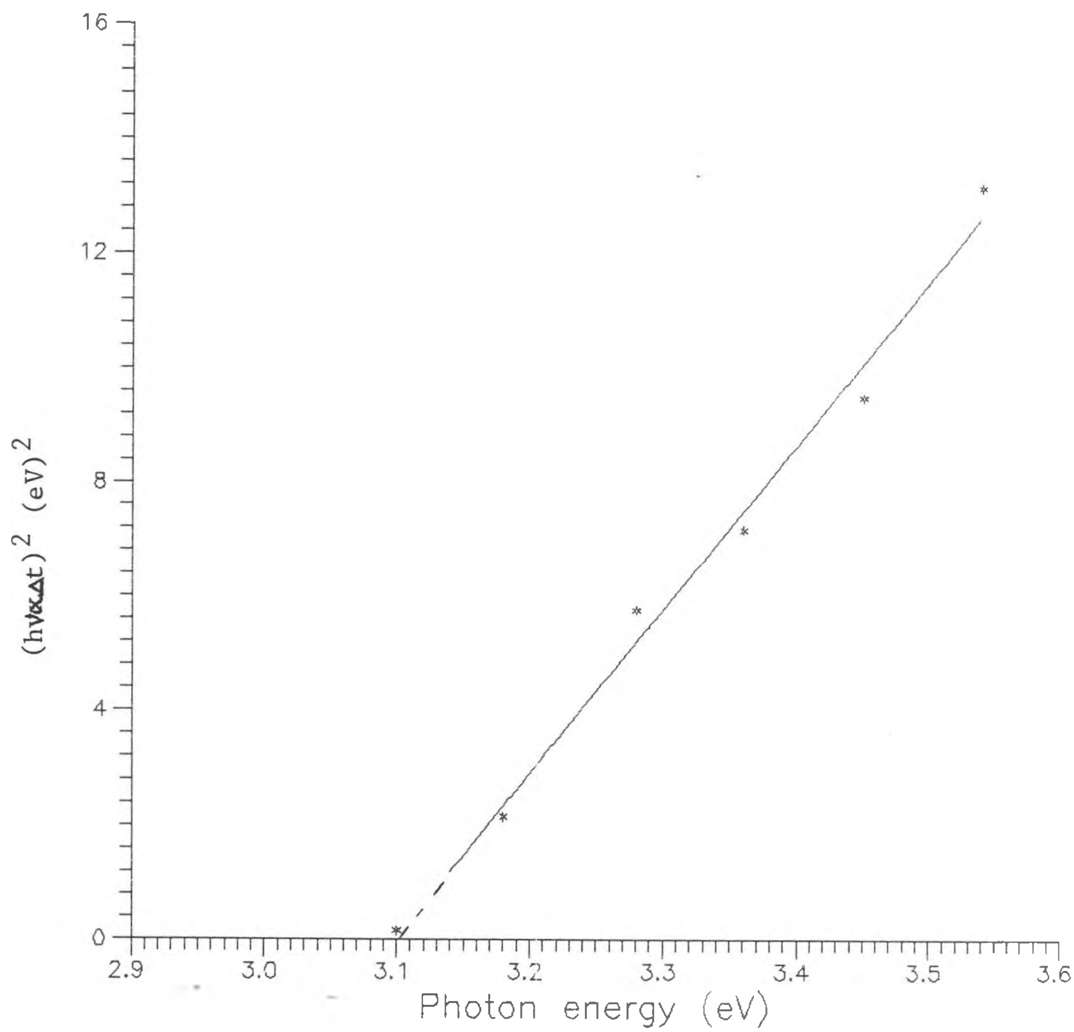

Fig. 5.10 : Determination of bandgap

5.4 Anealing Studies

The gross effect of annealing in air and in vacuum are that the electrical resistivity increases on annealing in air and decreases on annealing in vacuum [6]. Fig. 5.11 shows the cyclic behavior of zinc stannate in vacuum and in air ambient. The sheet resistance of the as-deposited zinc stannate films was about 160 KΩ at 25 °C. The film was first heated in air to a temperature of about 120 °C, the sheet resistance increased to 1.2 MΩ/□ via curve a. The sample was next heated in vacuum (1.5 x 10^{-4} Torr) at fixed temperature of 120 °C, which led to a decrease in sheet resistance via curve b to approximately 10 KΩ. When the film was cooled in the air to 25 °C, the sheet resistance increased via curve c. The same film was again annealed in a vacuum as temperature raised to 120 °C over a period of one hour, the sheet resistance fell via curve d to 14 KΩ/□. Similar behavior was reported on ZnO:Al [22].

Air and vacuum annealing reverse the effect of one another enormously hence eliminating possibilities of significant structural changes. Chemsorption and adsorption of oxygen on zinc stannate films explains the sheet resistance behaviour shown in Fig. 5.11. Chemisorbed oxygen at grain boundaries is also expected in as-deposited films since the deposition was carried out in the air at a temperature of about 450 °C. However, vacuum annealing of an as-deposited or air-annealed

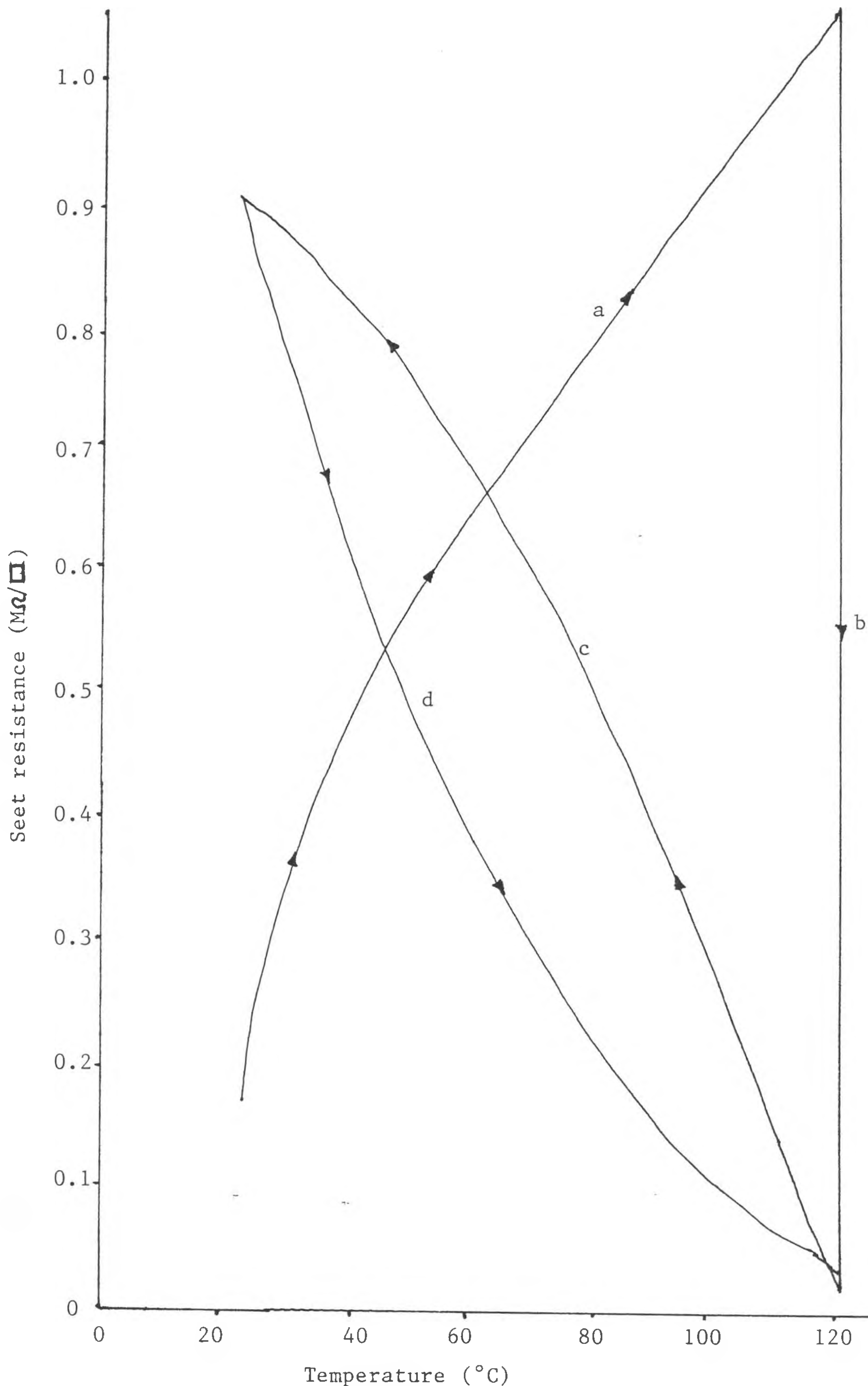

Fig. 5.11 : Variation in sheet resistance with temperature of zinc stannate films on annealing in different ambients. The annealing steps in chronological order were as labelled curves a-d, where the curves represent:
a - annealing in air with an increase in temperature
b - annealing in vacuum at constant temperature
c - cooling in air
d - annealing in vacuum with increase in temperature.

film lead to desorption of oxygen from the grain boundaries. The observed changes in resistivity of zinc stannate films on annealing can be attributed to the creation or annihilation of oxygen acceptor states at the grain boundaries which act as traps for electrons. Rapid increase in sheet resistance occur immediately the film is allowed to cool in air followed by a slower but much large increase. These effects are consistent with first, a surface effect followed by a slower change due to diffusion through the grain boundaries [15,22].

Using Table 4, Fig. 4.12 was drawn. Fig. 4.12 shows dependence of natural logarithm of sheet resistance on reciprocal temperature for vacuum annealed zinc stannate films. A linear behaviour and the relationship [27]

$$R_S = R_{si}\exp(E_a/k_BT) \qquad (5.5)$$

were observed. Where R_{si} is initial sheet resistance, E_a is the activation energy and k_B is the Boltzmann constant. Activation energies of about 0.43 eV and 0.083 eV were obtained using Fig. 5.12 and were attributed to the appearance of trapped states due to chemisorption of oxygen at zinc stannate grain boundaries.

Table 4 : Natural logarithm of sheet resistance and reciprocal of temperature for vacuum annealed zinc stannate.films.

T(K)	$[10^3/T](K^{-1})$	$R_s(K\Omega/\square)$	$\ln R_s$
303	3.3	7.8	2.05
323	3.1	7.0	1.94
343	2.92	6.2	1.82
353	2.83	5.5	1.70
363	2.75	5.0	1.61
368	2.72	4.6	1.53
373	2.68	3.8	1.36
381	2.62	2.9	1.06
383	2.61	2.4	0.88

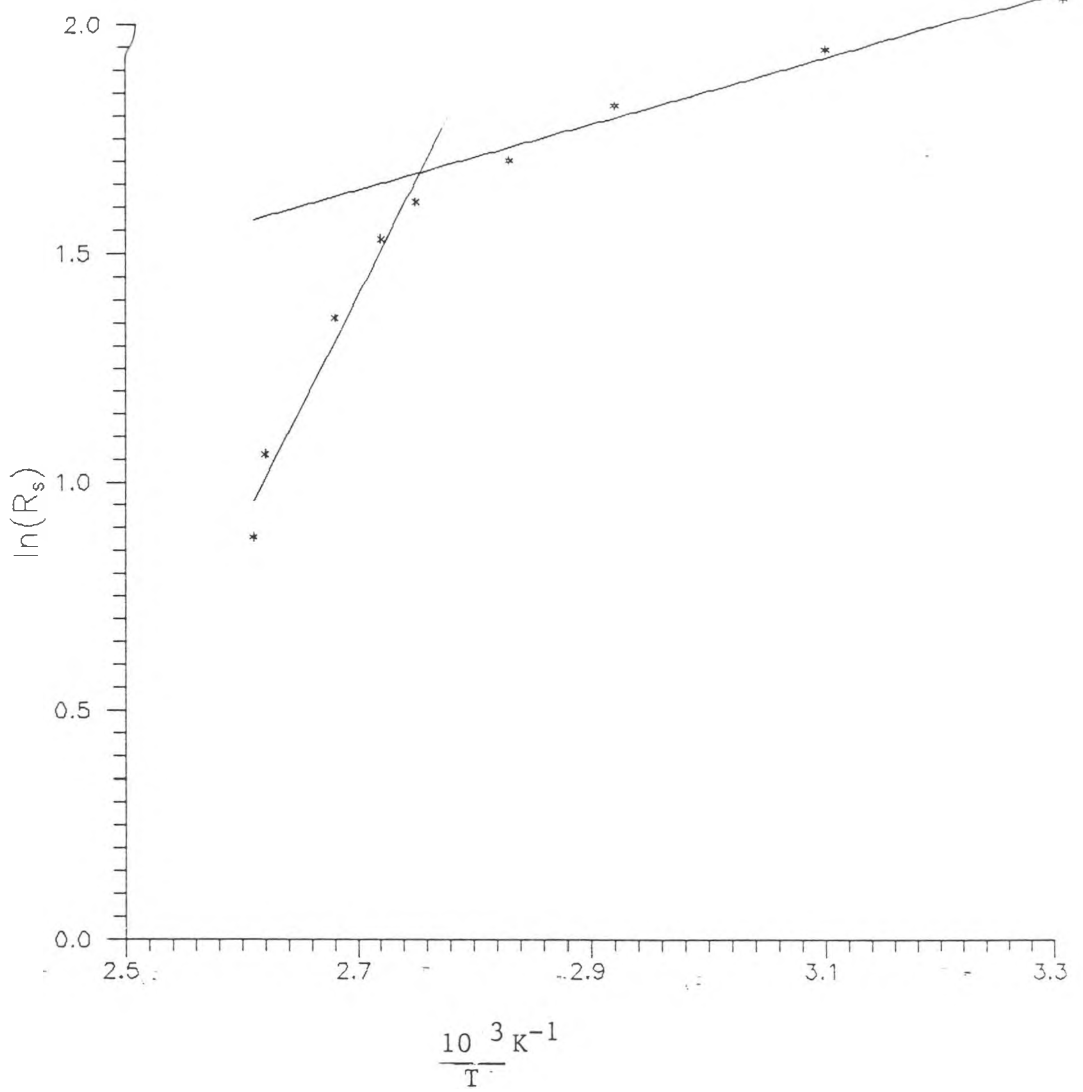

Fig. 5.12 : $\ln(R_s)$ Vs reciprocal temperature for zinc stannate films

5.5 Hall Effect Studies

Hall measurements show that Zn_2SnO_4 films are n-type semiconductors. Table 5 is given for the best three samples studied. The entries of table 5 were computed as shown in appendix C. Annealing in vacuum was done before Hall effect studies were conducted.

Table 5: Values of substrate temperature (T), resistivity (ρ), carrier concentration (N) and mobility (μ) for the best Zn_2SnO_4 sample studied.

T (°C)	$\rho \times 10^{-2}$ (Ωcm)	$N \times 10^{20}$ (cm^{-3})	μ (cm^2/Vs)
440	1.9	1.27	2.57
430	2.5	2.15	1.16
420	9.2	0.72	0.94

Generally, mobility was observed to increase with substrate temperature. The grain size increased with deposition temperature (see Fig. 5.3), causing a concurrent decrease in grain boundary scattering which in turn raised mobility. Similar results were reported for SnO_2 films [8].

5.6 Figure of Merit

The choice of a particular material is, in general, based on a set of performance requirements; these include electrical, optical, and mechanical properties as well as chemical stability. Common to all transparent conductor applications is the need for

optimizing the electrical and optical coating parameters. The optical and electrical properties of a transparent conductor coating are best characterized by the electrical sheet resistance R_s and optical transmission T_o.

A balance between transmission and sheet resistance can be achieved when the figure of merit is defined as [26]

$$\phi_{TC} = T^{x}/R_s \qquad (5.6)$$

where x=10 in order to simplify numerical calculations of practical figures of merit.

Using equation (5.6), the figure of merit for Zn_2SnO_4 was calculated and found to be approximately $1.72 \times 10^{-}$[illegible] $(K\Omega)^{-}$[illegible]. The less weight ϕ_{TC} places on R_s explains the relatively high figure of merit obtained for Zn_2SnO_4 films.

CHAPTER SIX

6. CONCLUSION AND SUGGESTION FOR FURTHER WORK

6.1 Conclusion

A mixture of two parts of 0.2 M solution of $ZnCl_2$ in isopropyl and water (volume ratio, 3:1) and one part of 0.2 M solution of $SnCl_4.5H_2O$ in butane-1-ol and water (volume ratio, 3:1) constituted the optimum precursor solution. A gas pressure of 7.5×10^4 Nm^{-2}, spray height of 30 cm, spray rate of 15 cm^3 per minute and a substrate temperature of 440 °C were established as the best Zn_2SnO_4 growth conditions.

The microcrystals of Zn_2SnO_4 films had a preferred orientation along c-axis normal to the surface, since only (002) diffraction peaks were observed. Scanning electron micrographs revealed that substrate temperature affects grain size i.e. film grown at 440 °C had bigger grain sizes than those grown at 380 °C.

Annealing in vacuum increased the carrier concentration due to the increase in the number of oxygen vacancies.

The optical band edge for zinc stannate was found to be around 400 nm wavelength. Transmission in the wavelength range 0.42 - 1.0 μm was found to be approximately 80%. Whereas the direct optical band gap was found to be 3.1 eV. Activation energies of about 0.43 eV and 0.83 eV were obtained and were attributed to the appearance of trapped states due to chemisorption of oxygen

at Zn_2SnO_4 grain boundaries. The best sample used for Hall effect studies gave a resistivity of 2.5×10^{-2} Ωcm, carrier concentration of 1.27×10^{20} cm^{-3} and mobility of 2.4 $cm^2/V.sec$.

6.2 Suggestions for Further Work.

The resistivity of Zn_2SnO_4 thin films is still high, therefore requires further optimization of growth parameters. Annealing at high temperatures in vacuum should be investigated since we never had a chance to anneal at temperatures above 120 ^0C despite the fact that resistivity was still reducing as temperature increased. It was difficult to grow uniform films by moving the hand slowly and keeping the spray height constant. An automatic system should be developed to take over manual movement of the sprayer. The durability and optical efficiency of Zn_2SnO_4 films should be investigated in photovoltaic and photothermal systems as low cost solar selective coatings.

REFERENCES

1. Agarwal M.P., "Solar Energy", S. Chand and Company Limited, New Delhi 1985, p. 4
2. Agnihotri O.P. and Gupta B.K., "Solar selective surfaces", Wiley, New York 1981. p 7-15
3. Yasuhiro Igasaki and Hiromi Santo, J.Appl. Phys. 69 (4), 1991. p 2190-2195
4. Jeong J.I., Moon J.H., Hong J.H, kang J.S., and Lee Y.P., Appl. Phys. Lett. 64 (10), 1994. p 1215-1217
5. Takada Synichi, J. Appl. Phys. 73 (15), 1993. p 4739-4742
6. Shigesato Y., Hayashi Y. and Haranoh T., Appl. Phys.Lett. 61 (1), 1992. p 1760
7. Granqvist C.G., " Material Science for solar Energy conversion systems", Pergamon Press, London. p 43
8. Shanthi E., Dutta V., Banerjee A. and chopra K.L., J. Appl. Phys. 51 (12), 1980. p 6243-6250
9. Kameswara L. and Vinni V., Appl. Phys. Lett. 63 (5), 1993. p 608 - 610
10. Abass A.K. and Mohammed M.T., J. Appl. Phys. 59 (5), 1986. p 1641-1642
11. Goyal D.J., Chitra Agashe and Marathe B.R., J. Appl. Phys. 73 (11), 1993. p 7520-7523
12. Quaranta Fabio, J. Appl. Phys. 74 (1), 1993. p 244-248
13. Yoonkee kim and Hunt W.D., J. Appl Phys. 76 (3), 1994. p 1455-1461
14. Yoonkee K., Fredrick S., and Robert J., J. Appl Phys. 75 (11), 1994. p 7299-7303

15. Roth A.P. and Williams D.F., J. Appl Phys. 52 (11), 1981. p 6685-6691

16. Hirotoshi S. and Tadatsugu M., J.Appl. Phys. 75 (3), 1994. p 1405-1409

17. Zielinski E.M., Vinci R.P., and Bravman J.C., J. Appl. Phys.76 (8), 1994. p 4516-4523

18. Hong Koo Kim and Michelle Mathur, Appl. Phys. Lett. 61 (21), 1992. p 2524-2526

19. Cavicchi R.E. and Antonik M.D.,Appl. Phys. Lett. 61 (16), 1992. p 1921-1923

20. Weber A., Sutter P., and Kanel Von H., J. Appl phys. 75 (11), 1994. p 7448-7455

21. Kunz R.R., Rothschild M., and Ehrlich D.J., Appl. Lett. 54 (17), 1989. p 2406

22. Sze S.M., " Physics of Semiconductor Devices" Wiley and Sons, New York 1969. p 34-80

23. Runyan W.P., "Semiconductor Measurements and Instruments", McGraw-Hill Kogakusha Ltd., (International Student Edition), London 1990. p 62

24. Rao B.V.N., " Mordern Physics", Wiley Eastern Ltd. 1992, New Delhi, p 396-399

25. JCPD, "Inorganic Phases" International Centre for Diffraction Data (1980). New York. p 571

26. Haacke G., J. Appl. Phys. 47 (9) 1976. p 4086-4089

27. Njoroge W.K., M.Sc. Thesis, Kenyatta University 1993, Unpublished.

28. Morgan D.V. and Board K., "An Introduction to Semiconductor Microtechnology", Second Edition, John Wiley and Sons, London 1990. p 18

29. James W. Mayer and Lau S.S., "Elecronic Materials Science", Maxwell Macmillan (Internation Edition), New York 1994. p 92-103

30. Walukewicz, Appl. Phys. Lett. 54 (21) 1989. p 2094-2096

31. Mittal K.L., "Particals on Surface, Detection, Adhession and Removal", Plenum Press, New York 1985. P 44

32. Adir Bar-Lev, "Semiconductors and Electronic Devices", Second Edition,Prentice Hall International 1984. p 74-76

33. Smith, "Semiconductors", Cambridge University press, London 1959. p 360

34. Tudore E. Jenkins, "Semiconductor Science", Prentice Hall International Limited, London 1995. p 276

APPENDIX A

Film Thickness Calculations

$$t = m_n\lambda_o\lambda_m/2n_r(\lambda_m-\lambda_o)\cos\phi \qquad (i)$$

where t is film thickness, λ_o is the wavelength at first maximum, λ_m is the wavelength at successive maxima, m_n is the number of maxima from λ_o to λ_m, ϕ is the angle of incidence of the beam as it hits the lower reflecting surface and n is the refractive index.

For n_r=2, m_n=1, λ_o=669 nm, λ_m=747.5 nm and ϕ=0

substituting in equation (i) above we obtain

$t = (1)(669)(747.5)/2(2)(747.5 - 669)\cos(0)$

$t = 0.16$ μm

All thickness calculations were done as shown in this example.

APPENDIX B

Absorption Coefficient Calculations

When reflection is neglected, transmission (T_o) is given by

$T_o = \exp(-\alpha t)$ (i)

where α is the absorption coefficient and t is the film thickness.

Therefore when α is made the subject of the formula, equation (i) becomes

$\alpha = -\text{In}T_o/t$ (ii)

For $t=(1592.6 \times 10^{-8})$ cm and $T_o=0.022$, substituted in equation (ii) gives

$\alpha = \{-\text{In}(0.022)/1592.6 \times 10^{-8}\}\ \text{cm}^{-1}$

$= \{2.3865295 \times 10^{-3} \times 10^{8}\}\ \text{cm}^{-1}$

$= 2.4 \times 10^{\text{[illegible]}}\ \text{cm}^{-1}$

This is the first absorption coefficient value given in Table 1. The rest of absorption coefficient values were calculated similarly as shown in this example.

APPENDIX C

Hall Effect Studies Calculations

Table 6 : Hall effect data and results for Zn_2SnO_4 thin films grown at different substrate temperatures.

T °C	I_y mA	V_H mV	R_H $\Omega cm^3/Vs$	N $x10^{20} cm^{-3}$	μ cm^2/Vs	ρ x10^-[illegible] Ωcm
440	0.4	-4.2	-0.049	1.27	2.58	1.9
430	0.4	-3.1	-0.029	2.15	1.16	2.5
420	0.1	-2.9	-0.086	0.72	0.94	9.2

The negative sign in the table above appears due to the fact that the carriers are electrons. Films deposited at substrate temperatures below 420 °C had very high sheet resistance which attributed to the failure to obtain any significant data from them during Hall effect studies.

Taking the sample prepared at substrate temperature of 440 °C as an example, the entries in table 5 were computed using the data below obtained from measurements.

magnetic flux density, B_z = 4.4×10^{-3} Wb.cm^{-2}

film thickness, t = 0.16 μm

sheet resistance value, R_s = 1.2 KΩ/□

length of the square sample, $d = 1.0$ cm

current flow in y-plane, $I_y = 0.4$ mA

Hall voltage, $V_H = -4.2$ mV

Resistivity (ρ) is given by

$$\rho = R_s t$$

$$= 1.2 \times 10^{-3} \times 1.6 \times 10^{-5}\ \Omega cm$$

$$= 1.9 \times 10^{-2}\ \Omega cm$$

Current density (J_y) is given by

$J_y = I_y/A$, where A is surface area.

$$= (0.4 \times 10^{-3})/(1.0 \times 1.6 \times 10^{-5})$$

$$= 19.5\ Acm^{-2}$$

The Hall coeficient (R_H) is given by

$$R_H = E_x/J_y B_z$$

$$R_H = (-4.2 \times 10^{-3})/(19.5 \times 4.4 \times 10^{-3})$$

$$= -0.049\ \Omega cm/V.sec^{-1}$$

Carrier concentration (N) is given by

$$\mathbf{N} = 1/R_H q$$

$$= 1/(0.049 \times 1.6 \times 10^{-19})$$

$$= 1.27 \times 10^{20}\ cm^{-3}$$

Conductivity (σ) is given by

$$\sigma = 1/\rho$$

$$= 1/(1.9 \times 10^{-2})$$

$$= 52.6\ \Omega^{-1}\text{cm}^{-1}$$

Mobility (μ) is given by

$$\mu = R_H\sigma$$

$$= 0.049 \times 52.6$$

$$= 2.58\ \text{cm}^2/\text{V.sec.}$$